

# Random SU(2)-symmetric spin- $S$ chains

V. L. Quito,<sup>1</sup> José A. Hoyos,<sup>2</sup> and E. Miranda<sup>1</sup>

<sup>1</sup>*Instituto de Física Gleb Wataghin, Unicamp, Rua Sérgio Buarque de Holanda, 777, CEP 13083-859 Campinas, SP, Brazil*

<sup>2</sup>*Instituto de Física de São Carlos, Universidade de São Paulo, C.P. 369, São Carlos, SP 13560-970, Brazil*

(Dated: August 8, 2016)

We study the low-energy physics of a broad class of time-reversal invariant and SU(2)-symmetric one-dimensional spin- $S$  systems in the presence of quenched disorder via a strong-disorder renormalization-group technique. We show that, in general, there is an antiferromagnetic phase with an emergent SU( $2S+1$ ) symmetry. The ground state of this phase is a random singlet state in which the singlets are formed by pairs of spins. For integer spins, there is an additional antiferromagnetic phase which does not exhibit any emergent symmetry (except for  $S=1$ ). The corresponding ground state is a random singlet one but the singlets are formed mostly by trios of spins. In each case the corresponding low-energy dynamics is activated, i.e., with a formally infinite dynamical exponent, and related to distinct infinite-randomness fixed points. The phase diagram has two other phases with ferromagnetic tendencies: a disordered ferromagnetic phase and a large spin phase in which the effective disorder is asymptotically finite. In the latter case, the dynamical scaling is governed by a conventional power law with a finite dynamical exponent.

PACS numbers: 75.10.Jm, 75.10.Pq, 75.10.Nr

## I. INTRODUCTION

Systems with random interactions comprise an important research field in condensed matter physics. At the same time that some disorder is unavoidable in experiments, its presence can completely change the long wavelength behavior of the system, driving it through quantum phase transitions (for a review see, e. g., references 1–3). Remarkably, the novel low-energy behavior of matter that appears in the strong-disorder limit is typically very distinct from that of the clean systems. A striking example is the low-energy behavior of one-dimensional random spin chains. For sufficiently strong randomness, the ground state of the antiferromagnetic (AF) Heisenberg spin- $S$  chain becomes a collection of nearly independent singlets of spin pairs [see Fig. 2(a)]: the so-called random singlet state.<sup>4</sup> The energy spectrum associated with these singlets is extremely broad and is responsible for singular response functions. The magnetic susceptibility  $\chi$ , for instance, diverges as  $\sim (T \ln^{1/\psi} T)^{-1}$ , with a universal (disorder-independent) tunneling exponent  $\psi = 1/2$ . In addition, the typical and average spin-spin correlation functions behave quite differently. While the former one decays as a stretched exponential  $\sim e^{-r^\psi}$ , where  $r$  is the distance between the spin in convenient units, the latter decays much more slowly, as a power law  $\sim r^{-4\psi}$ . The fact that typical and average values differ so much is the hallmark of phases governed by infinite-randomness fixed points, a concept that could only be grasped after the development of a strong-disorder renormalization-group (SDRG) method.<sup>5–7</sup> In this method, one keeps track of the entire effective distribution of energy and length scales under the renormalization group (RG) coarse graining. In the vicinity of an infinite-randomness fixed point these distributions tend to become infinitely broad along the RG flow.

Later on, it was realized that very similar behavior

would also appear in other random spin chains, namely, at multicritical points of dimerized spin- $S$  chains,<sup>8</sup> in AF SU( $N$ ) spin chains,<sup>9</sup> and in non-abelian anyonic SU(2) <sub>$k$</sub>  spin chains.<sup>10</sup> The difference is that  $\psi$  now depends on other model details. In the first model, the tunneling exponent is  $\psi = 1/N_1$ , where  $N_1$  is the number of dimerized phases meeting at the multicritical point (the maximum being  $2S+1$ ). In the second model,  $\psi = 1/N_2$  where  $N_2$  is the number of different spin representations describing the effective spin degrees of freedom (the maximum being  $N$ ). In the third model,  $\psi = 1/N_3$  where  $N_3 = k$ . In addition, the ground state of these models is distinct from the usual pairwise random singlet state because the singlets are now formed by a larger number of spins, such as spin trios, quartets and so on [see Fig. 2(b)].

Recently,<sup>11</sup> we have shown that random spin-1 chains with bilinear and biquadratic SU(2)-symmetric interactions harbor two types of random singlet phases: one in which the spin singlets are formed by spin pairs and characteristic tunneling exponent  $\psi = 1/2$ , and another in which the spins are made in the great majority of spin trios. In addition,  $\psi = 1/3$ . More interestingly, these phases exhibit emergent SU(3) symmetry.

Despite all these developments, we still do not have a simple criterion to decide whether a given random spin chain model is in a certain random singlet phase, or whether the random singlet state has an emergent symmetry. In this paper, we investigate the most general SU(2)-symmetric random spin- $S$  model with nearest-neighbor time-reversal-symmetric interactions only. We show that, in the strong disorder limit, these random singlet states are realized in this model. In general there is a random singlet phase where the singlets are formed by spin pairs only and the corresponding universal exponent  $\psi = \frac{1}{2}$ . Strikingly, this pairwise random singlet exhibits an emergent SU( $2S+1$ ) symmetry. We show that this phase is characterized not by one, but rather

by  $2S$  stable fixed points associated with the same pairwise random singlet state. The difference between them stems only from the structure of the low-energy excitations, which are all deformations of the spectrum with exact  $SU(2S+1)$  symmetry. Furthermore, the presence of additional  $SU(2)$ -invariant couplings (with increasing powers of the scalar products of spin operators) helps stabilize these phases, providing them with a large basin of attraction.

In addition to this pairwise random singlet phase, we show that integer spin- $S$  chains possess also another random singlet phase in their phase diagram. This state is formed by spin trios and other multiples of three, although in much less quantity, see Fig. 2(b). Besides, it exhibits a universal exponent  $\psi = \frac{1}{3}$ . For  $S = 1$ , this state exhibits emergent  $SU(3)$  symmetry. For higher integer spins, there is no such symmetry enhancement.

The experimental relevance of systems with a large number of internal degrees of freedom stems from the possibility of their realization in condensed matter systems or, more promisingly, in cold-atom systems loaded in optical lattices. Candidates include alkali bosons, such as  $^{23}\text{Na}$  and  $^{87}\text{Rb}$ , as well as alkali ( $^{132}\text{Cs}$ ) or alkaline-earth fermions ( $^9\text{Be}$ ,  $^{135}\text{Ba}$ ,  $^{137}\text{Ba}$ ,  $^{87}\text{Sr}$  or  $^{173}\text{Yb}$ ). In the Mott insulating limit, the importance of spin-spin interactions beyond the Heisenberg term has been discussed for these systems.<sup>12–15</sup> Furthermore, in some cases the systems possess a symmetry larger than the usual  $SU(2)$ . For example, in the case of spin- $\frac{3}{2}$  fermions, an exact  $SO(5)$  symmetry has been discovered which requires no fine-tuning.<sup>13,15</sup> In the case of alkaline-earth atoms, the total spin is of purely nuclear origin and is decoupled from the remaining dynamics. It thus provides the internal degrees of freedom that realize an  $SU(N)$  symmetry,<sup>16,17</sup> as in the cases of  $^{87}\text{Sr}$  ( $N = 10$ )<sup>18</sup> or  $^{173}\text{Yb}$  ( $N = 6$ ).<sup>19</sup> An  $SU(6)$  Mott insulating state of  $^{173}\text{Yb}$  atoms has been achieved,<sup>20</sup> although lowering the temperature below the spin-exchange scale remains a challenge. Two of us have already analyzed disordered  $SU(N)$ -symmetric chains.<sup>9</sup> The phases we will discuss include these enhanced symmetry points, as well as others, as we will discuss.

The present manuscript is structured as follows. First, in Section II, we present the model and introduce the irreducible spherical tensor notation in which our RG treatment is more natural. We also make a connection with the projector notation which is often used by the cold-atom community. The decimation steps of the SDRG procedure are derived in Section III. This generalizes the methods of Ref. 21 from the generic random spin- $S$  Heisenberg chain to the generic random spin- $S$  time-reversal and  $SU(2)$ -symmetric chain. We then provide a summary of the results of the RG flow in Sec. IV. In Section V, we discuss the RG fixed point structure. We determine that a phase exists which has a random singlet ground state with emergent  $SU(2S+1)$  symmetry. We also find the other fixed point which happens only for integer spin- $S$  chains. Finally, we briefly mention other fixed points with FM tendencies. In Secs. VI and VII,

we apply in detail our framework to the particular cases of spin- $\frac{3}{2}$  and spin-2 chains, respectively. A less technical summary of our main results is given in Sec VIII. In Sec. IX we give a final summary and discuss future directions that remain to be explored. Much of our more technical developments are described in several Appendices.

## II. MODEL

A broad class of disordered time-reversal and  $SU(2)$  symmetric spin- $S$  Hamiltonians of a linear chain of  $N_{\text{sites}}$  sites (with periodic boundary conditions) can be written as

$$H = \sum_{i=1}^{N_{\text{sites}}} \sum_{J=0}^{J_{\text{max}}} \alpha_i^{(J)} (\mathbf{S}_i \cdot \mathbf{S}_{i+1})^J, \quad (1)$$

where  $\mathbf{S}_i = (S_i^x, S_i^y, S_i^z)$  are the usual spin- $S$  operators at site  $i$ ,  $\alpha_i^{(J)}$  are exchange couplings that are taken to be independent random variables distributed with the probability distributions  $\bar{P}_J(\alpha)$ . The maximum power  $J_{\text{max}}$  for a spin- $S$  system is  $2S$ , since larger powers of the spin operators can be written as linear combinations of smaller ones.

For our renormalization-group transformations, it will be convenient to rewrite the Hamiltonian in Eq. (1) in terms of irreducible spherical tensors (ISTs)  $Y_{J,M}(\mathbf{S}_j)$  instead of powers of spin operators  $S^k$ .<sup>22</sup> The ISTs can be defined via their commutation relations with the spin operators (page 71 of Ref. 23)

$$[S_i^\pm, Y_{J,M}(\mathbf{S}_j)] = \sqrt{J(J+1) \mp M(1 \pm M)} \times Y_{J,M \pm 1}(\mathbf{S}_i) \delta_{i,j}, \quad (2)$$

$$[S_i^z, Y_{J,M}(\mathbf{S}_j)] = M Y_{J,M}(\mathbf{S}_i) \delta_{i,j}. \quad (3)$$

Here,  $Y_{J,M}(\mathbf{S}_i)$  is an IST of rank  $J$  with  $2J+1$  components ( $M = -J, -J+1, \dots, J-1, J$ ) and they are functions of the spin operators  $\mathbf{S}_i$ . From these commutation relations, a recipe to construct them immediately follows. The idea is to start with the operator of highest  $M$ ,

$$Y_{J,M=J}(\mathbf{S}_i) \propto (S_i^+)^J, \quad (4)$$

and make use of the commutation relations (2) to lower the component index

$$Y_{J,M-1}(\mathbf{S}_i) = \frac{[S_i^-, Y_{J,M}(\mathbf{S}_i)]}{\sqrt{J(J+1) - M(M-1)}}. \quad (5)$$

Note that these ISTs resemble the spherical harmonics  $\mathcal{Y}_{J,M}(\mathbf{r})$ . There is, however, an important difference: if one wishes to “promote” spherical harmonics to ISTs,

symmetrization is often required. For instance,  $\mathcal{Y}_{1,0} \propto \frac{z}{r}$  is promoted to  $Y_{1,0} \propto S^z$ , but the  $\frac{xz}{r^2}$  term of the spherical harmonic  $\mathcal{Y}_{2,1}$  is promoted to  $\frac{1}{2}(S^z S^x + S^x S^z)$ . Since the operator in Eq. (4) is already symmetrized, the recursive application of Eq. (5) automatically leads to symmetrized IST operators. We will also use the same IST normalization of Ref. 23 (page 23).

There is another interesting aspect we wish to point out. The spin operators themselves are obviously rewritten as first-rank ISTs. For example,  $S^z \propto Y_{1,0}$  and  $S^x \propto (Y_{1,-1} - Y_{1,1})$ . The dyadic term  $S^x S^x$ , however, is not, as it mixes ISTs of different ranks. It has one component  $\propto [Y_{1,-1}, Y_{1,1}] \propto Y_{1,0}$  and another component  $\propto Y_{1,1}^2 \propto Y_{2,2}$ . Evidently, the former component transforms as a vector while the latter one transforms as a second-rank tensor. Therefore, each power  $(\mathbf{S}_i \cdot \mathbf{S}_{i+1})^J$  appearing in the Hamiltonian (1) transforms as linear combinations of tensors of ranks  $J' \leq J$ . Rewriting (1) in terms of ISTs allows us to untangle the different ranks. As we shall see, this is of fundamental importance for the analysis of the SDRG flow.

We now come to the point of rewriting the Hamiltonian with this new set of operators. The important step is to build rotation-invariant two-site terms. We define the operator  $\hat{O}_J$  as the scalar product of IST operators of the same rank (page 72 of Ref. 23)

$$\hat{O}_J(\mathbf{S}_i, \mathbf{S}_{i+1}) \equiv \sum_{M=-J}^J (-1)^M Y_{J,M}(\mathbf{S}_i) Y_{J,-M}(\mathbf{S}_{i+1}). \quad (6)$$

One can explicitly check using Eqs. (2) and (3) that

$$[S_i^\pm + S_{i+1}^\pm, \hat{O}_J] = [S_i^z + S_{i+1}^z, \hat{O}_J] = 0, \quad (7)$$

which shows that  $\hat{O}_J$  is indeed rotation-invariant. For example, the operator  $\hat{O}_2$  is<sup>22</sup>

$$\begin{aligned} \hat{O}_2(\mathbf{S}_i, \mathbf{S}_{i+1}) &= \frac{15}{16\pi} (\mathbf{S}_i \cdot \mathbf{S}_{i+1}) + \frac{15}{8\pi} (\mathbf{S}_i \cdot \mathbf{S}_{i+1})^2 \\ &\quad - \frac{5}{8\pi} \mathbf{S}_i^2 \mathbf{S}_{i+1}^2. \end{aligned} \quad (8)$$

In Appendix A, we list all the  $\hat{O}_J$ 's needed in this paper. The Hamiltonian in Eq. (1) can thus be rewritten as

$$H = \sum_i H_{i,i+1} = \sum_{i=1}^{N_{\text{sites}}} \sum_{J=0}^{J_{\text{max}}} K_i^{(J)} \hat{O}_J(\mathbf{S}_i, \mathbf{S}_{i+1}). \quad (9)$$

Obviously, the new coupling constants  $K_i^{(J)}$  are linear combinations of the original  $\alpha_i^{(J)}$  and vice-versa (see Appendix A). Additionally, the distributions  $\bar{P}_J(\alpha)$  determine the distributions of  $K_i^{(J)}$ ,  $\mathcal{P}_J(K)$ . In this paper, we always work directly with  $\mathcal{P}_J(K)$ .

A third important form of the Hamiltonian involves the use of projection operators onto states of well-defined total angular momentum  $\tilde{S}$  of each pair of sites. The latter can be written for a pair of spins as (page 38 of Ref. 23)

$$P_{\tilde{S}}(\mathbf{S}_i, \mathbf{S}_{i+1}) = \prod_{\sigma \neq \tilde{S}} \frac{2\mathbf{S}_i \cdot \mathbf{S}_{i+1} + 2S(S+1) - \sigma(\sigma+1)}{\tilde{S}(\tilde{S}+1) - \sigma(\sigma+1)} \quad (10)$$

$$= \sum_{M=-\tilde{S}}^{\tilde{S}} |\tilde{S}M\rangle \langle \tilde{S}M|, \quad (11)$$

where  $\sigma = |S_i - S_{i+1}|, \dots, S_i + S_{i+1}$ . It is clear that  $P_{\tilde{S}}(\mathbf{S}_i, \mathbf{S}_{i+1})$  selects, from all possible states of total angular momentum of the pair, only the one equal to  $\tilde{S}$ . The generic SU(2)-symmetric term for a pair of spins can thus be written as a linear combination of these projectors and

$$H = \sum_i \sum_{J=0}^{J_{\text{max}}} \epsilon_i^{(J)} P_J(\mathbf{S}_i, \mathbf{S}_{i+1}). \quad (12)$$

This third form is common when the spin Hamiltonian describes the low-energy sector of cold-atom systems in optical lattices at commensurate fillings. In such cases, if only *s*-wave scattering is retained, then  $\epsilon_i^{(J)} = 0$  for odd  $J$ , as required by the (anti)-symmetry of the wave function of a pair of (fermionic) bosonic atoms<sup>15,24</sup>. Linear transformations between  $\epsilon_i^{(J)}$ ,  $K_i^{(J)}$  and  $\alpha_i^{(J)}$  are given in Appendix A.

For convenience, in Table I, we summarize the notation we use throughout the paper.

### III. METHOD: STRONG DISORDER RENORMALIZATION GROUP

In this section, we derive the RG decimation procedure for the Hamiltonian in Eq. (9). The basic idea of the strong-disorder RG is to progressively eliminate *local* high-energy degrees of freedom while at the same time keeping the low-energy physics unchanged<sup>5-7</sup>. The local energy scales  $\Delta_i$  are the local gaps of the Hamiltonian  $H_{i,i+1}$  describing the coupling between spins  $S_i$  and  $S_{i+1}$ . We first find the largest gap  $\Omega = \max\{\Delta_i\}$ , which sets the RG scale. Let us say that  $\Omega = \Delta_2$ . We keep the ground multiplet of spins  $S_2$  and  $S_3$  and remove the higher-energy ones. Focusing on the four-spin Hamiltonian

$$H_{4\text{sites}} = H_{1,2} + H_{2,3} + H_{3,4}, \quad (13)$$

Description	Notation
Coupling constant of the term $(\mathbf{S}_i \cdot \mathbf{S}_{i+1})^n$ [see Eq. (1)]	$\alpha_i^{(n)}$
Irreducible spherical tensor of rank $J$ , component $M$ , for a spin $\mathbf{S}$	$Y_{J,M}(\mathbf{S})$
Coupling constant of the term $\hat{O}_J(\mathbf{S}_i, \mathbf{S}_{i+1})$ [see Eq. (9)]	$K_i^{(J)}$
Projector onto a multiplet of total angular momentum $\tilde{S}$ of the pair of spins $\mathbf{S}_i, \mathbf{S}_{i+1}$ [see Eq. (10)]	$P_{\tilde{S}}(\mathbf{S}_i, \mathbf{S}_{i+1})$
Coupling constant of the term $P_J(\mathbf{S}_i, \mathbf{S}_{i+1})$ [see Eq. (12)]	$\epsilon_i^{(J)}$

Table I. A summary of the notation used in this paper.

we then treat  $H_{1,2} + H_{3,4}$  as a perturbation to  $H_{2,3}$ . The procedure is iterated until we reach the low energy scale of interest. Essentially two cases must be distinguished, according to whether the eliminated multiplet is degenerate or not. Next, we outline these two possible RG decimation steps. Some details of the derivation are relegated to Appendix B.

### 1. First-Order Perturbation Theory

In the case when the lowest energy multiplet of the two-site problem is not a singlet, it is generally sufficient to treat the effect of  $H_{1,2} + H_{3,4}$  via first-order perturbation theory. If the ground multiplet of spins  $S_2$  and  $S_3$  has total angular momentum  $\tilde{S}$  we can replace  $S_2$  and  $S_3$  by a new effective spin  $\tilde{S}$ . The renormalized couplings  $\tilde{K}_{1,3}^{(J)}$  between  $\tilde{S}$  and  $S_{1,4}$  are then obtained by projecting  $H_{1,2} + H_{3,4}$  onto this degenerate ground state. It is important to note that the projected Hamiltonian has the same functional form as the unperturbed one. See Fig. (1) (“1st order” case) for a graphical representation of the procedure in this case.

Let us show in more detail how  $\tilde{K}_1^{(J)}$  and  $\tilde{K}_3^{(J)}$  can be found. Projecting  $H_{1,2}$  onto the multiplet  $\tilde{S}$  (similarly for  $H_{3,4}$ ), we obtain

$$\tilde{H}_{1,2} = P_{\tilde{S}} H_{1,2} P_{\tilde{S}} = \sum_{J=0}^{J_{\max}} K_1^{(J)} \sum_{M=-J}^J (-1)^M \quad (14)$$

$$\times Y_{JM}(\mathbf{S}_1) P_{\tilde{S}} Y_{J-M}(\mathbf{S}_2) P_{\tilde{S}} \quad (15)$$

$$= \sum_{J=0}^{J_{\max}} \tilde{K}_1^{(J)} \sum_{M=-J}^J (-1)^M Y_{JM}(\mathbf{S}_1) Y_{J-M}(\tilde{\mathbf{S}}) \quad (16)$$

$$= \sum_{J=0}^{J_{\max}} \tilde{K}_1^{(J)} \hat{O}_J(\mathbf{S}_1, \tilde{\mathbf{S}}), \quad (17)$$

where  $P_{\tilde{S}}$  is the projector in Eq. (10). The step from (15) to (16) involves the application of the Wigner-Eckart theorem:  $P_{\tilde{S}} Y_{J-M}(\mathbf{S}_2) P_{\tilde{S}} = f^{(J)}(S_2, S_3, \tilde{S}) Y_{J-M}(\tilde{\mathbf{S}})$ , where the constant  $f^{(J)}$  does not depend on  $M$ . The last feature preserves the SU(2) symmetry. Therefore, the neighboring couplings  $K_1^{(J)}$  and  $K_3^{(J)}$  are renormalized

to

$$\begin{aligned} \tilde{K}_1^{(J)} &= f^{(J)}(S_2, S_3, \tilde{S}) K_1^{(J)}, \\ \tilde{K}_3^{(J)} &= f^{(J)}(S_3, S_2, \tilde{S}) K_3^{(J)}, \end{aligned} \quad (18)$$

while the set of couplings  $\{K_2^{(J)}\}$  is removed. This is a generalization to higher-order ISTs of the RG step derived by Westerberg *et al.* in Ref. 21. In Appendix (B), we obtain closed-form expressions for the functions  $f^{(J)}$  in terms of Wigner’s 6- $j$  symbols.

In the lowest rank case  $J = 1$ , i. e., for the usual Heisenberg Hamiltonian, the effective couplings are always nonzero (except in the obvious non-degenerate case  $\tilde{S} = 0$ ). Interestingly, this is not always true in the higher-rank cases. In fact, there are two cases where the above effective couplings can vanish:

*Case (a): If the IST rank  $J$  is larger than  $2\tilde{S}$ .* In this case, the projection is zero simply because one cannot construct a large rank- $J$  IST out of small angular momentum operators. A general derivation can be found in Appendix B. For example, when  $S_2 = S_3 = 3/2$  (thus,  $J_{\max} = 3$ ) and the ground multiplet has  $\tilde{S} = 1$ , the IST  $Y_{J=3,M}(\tilde{\mathbf{S}})$  vanishes identically. We will come back to this point in Sections VI and VII when we study the spin- $\frac{3}{2}$  and spin-2 chains;

*Case (b): If the function  $f^{(J)}$  vanishes for some specific combinations of  $S_2$ ,  $S_3$  and  $\tilde{S}$  not predicted by case (a).* For example, when  $S_2 = S_3 = \frac{3}{2}$  and  $J = \tilde{S} = 2$ ,  $f^{(J)}(S_2, S_3, \tilde{S}) = 0$ . Note that  $J < 2\tilde{S}$ , so case (a) does not apply. We can explicitly show that this case never happens for ISTs with  $J = 1$ . It is a feature that only happens when higher rank ISTs are included. Since there is no general rule to predict when it happens, its consequences have to be analyzed on a case-by-case basis.

Evidently, these two cases configure a failure of the usual RG decimation procedure since the renormalized constants vanish and the chain becomes disconnected from that spin pair and is effectively broken up. The remedy is to include corrections in higher orders of perturbation theory. This would introduce new types of terms in the effective Hamiltonian (such as 3-spin couplings), which makes the problem much harder to treat. In this paper, we do not implement this remedy in full generality, although we discuss some of its features in Appendix F. Nonetheless, as we discuss in Section VIC, the effects of



such peculiar decimations in the RG flow are not important in the great majority of flows. In general, first-rank couplings  $K^{(1)}$  are present and the chains never become disconnected.

Finally, we emphasize that we assume that two or more multiplets of well-defined angular momentum are not degenerate in the ground multiplet. If this were not the case, the projection from Eq. (15) to Eq. (16) would have to incorporate the projection onto the additional multiplets. In general, this procedure would change the functional form of the projected Hamiltonian and a more elaborate RG procedure would be needed. Nevertheless, these accidental degeneracies appear only by fine tuning of the coupling constants  $K_2^{(J)}$  and can be safely ignored. Such high-symmetry cases are unstable in the sense that the RG flow is always away from them. We will come back to this point later when we analyze a few cases of physical importance.

## 2. Second-Order Perturbation Theory for singlets

When the two-spin problem has a singlet ground state, the first-order perturbation theory term vanishes and a second-order perturbation analysis is necessary. In this case, the spin pair  $S_2$  and  $S_3$  is frozen into a singlet and decouples from the chain, while the neighboring spins  $S_1$  and  $S_4$  become connected (due to virtual excitations of the singlet) via new effective couplings not present in the initial Hamiltonian. This is depicted in Fig. (1) as the “2nd order” case.

Let us define  $S \equiv S_2 = S_3$ , since a necessary condition for singlet formation is that the spins of the two sites are equal. The second-order perturbation-theory renormalization of the Hamiltonian is given by

$$\tilde{H}_{1,4} = P_0 (H_{1,2} + H_{3,4}) P_0 \frac{1}{E_0 - H_{2,3}} P_0 (H_{1,2} + H_{3,4}) P_0, \quad (19)$$

where  $E_0$  is the energy of the singlet,  $P_0$  is the projector onto the singlet state, and  $P_0 = 1 - P_0$  is the projector onto all other multiplets  $J' = 1, \dots, 2S$ . Neglecting unimportant constant terms, we get

$$\tilde{H}_{1,4} = P_0 H_{1,2} P_0 \frac{1}{E_0 - H_{2,3}} P_0 H_{3,4} P_0 + \text{H.c.} \quad (20)$$

$$= 2 P_0 H_{1,2} P_0 \frac{1}{E_0 - H_{2,3}} P_0 H_{3,4} P_0. \quad (21)$$

Writing  $H_{1,2}$  and  $H_{3,4}$  explicitly, we are left with the challenge of computing terms like  $P_0 Y_{J-M}(\mathbf{S}) P_0$ . Let us denote by  $J' \neq 0$  an arbitrary total angular momentum present in the projection operator  $P_0$ . The Wigner-Eckart theorem (page 74 of Ref. 23) ensures the only value of  $J'$  yielding a non-zero matrix element is  $J' = J$ , that is,  $\langle 00 | Y_{J-M}(\mathbf{S}) | J'M' \rangle \propto \delta_{J,J'} \delta_{M,M'}$ . Therefore, only the total angular momentum equal to

the IST rank gives a non-vanishing contribution to the perturbation theory. By defining  $\tilde{J}_{\max} = \min(J_{\max}, 2S)$ , and  $\Delta E(0, J) < 0$  to be the energy difference between the ground state and the excited state of total angular momentum  $J$ , we get

$$\tilde{H}_{1,4} = 2 \sum_{J=1}^{\tilde{J}_{\max}} K_1^{(J)} K_3^{(J)} \times \sum_{M=-J}^J \frac{(-1)^M g(S, J)}{\Delta E(0, J)} Y_{JM}(\mathbf{S}_1) Y_{J-M}(\mathbf{S}_4), \quad (22)$$

where

$$(-1)^M g(J, S) = \langle 00 | Y_{J-M}(\mathbf{S}) | JM \rangle \langle JM | Y_{JM}(\mathbf{S}) | 00 \rangle. \quad (23)$$

Note that neither the energy denominator  $\Delta E(0, J)$  nor the function  $g(J, S)$  depends on  $M$ , since the Hamiltonian is  $SU(2)$  symmetric. A closed-form expression for the function  $g(S, J)$  can be found in Appendix B, where the values needed in this paper are also listed. In conclusion, the effective Hamiltonian has the form

$$\tilde{H}_{1,4} = \sum_{J=1}^{\tilde{J}_{\max}} \tilde{K}_{14}^{(J)} \hat{O}_J(\mathbf{S}_1, \mathbf{S}_4), \quad (24)$$

where the renormalized couplings are

$$\tilde{K}_{1,4}^{(J)} = 2 \frac{g(J, S_2)}{\Delta E(0, J)} K_1^{(J)} K_3^{(J)}. \quad (25)$$

Eqs. (18) and (25) highlight the most important feature of the decimation procedure: under the RG flow, *the renormalized couplings  $\tilde{K}_{i,j}^{(J)}$  depend only on coupling constants of the same rank  $J$* , which is a direct consequence of the  $SU(2)$  symmetry. This is why working with the ISTs is a natural choice for these systems. This will have profound consequences for the identification of the stable fixed points, as will become clear later.

In summary, we have determined the decimation procedure for our generic  $SU(2)$ -symmetric quantum spin- $S$  chain (see schematics in Fig. (1)), which generalizes the one obtained by Westerberg *et al.*<sup>21</sup> devised to describe generic spin- $S$  Heisenberg chains (i.e., with  $J_{\max} = 1$ ). We search for the strongest coupled spin pair in the chain (which defines our RG cutoff energy scale  $\Omega$ ) and decimate it. If the local ground state is a singlet, the spin pair is removed and the renormalized coupling constants between the neighbor spins are given by Eq. (25). Otherwise, the spin pair is replaced by an effective spin  $\tilde{S}$  given by the total angular momentum of the ground-state multiplet. Moreover, this new effective spin degree

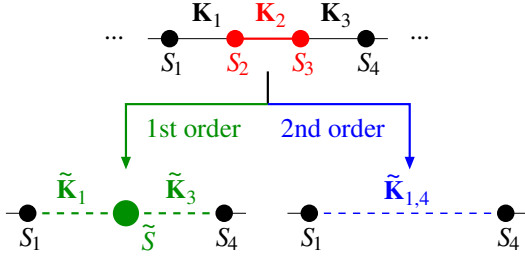


Figure 1. (Color online) Schematic decimation procedure. The decimated spins  $S_2$  and  $S_3$  are either replaced by an effective spin  $\tilde{S}$  (“1st order” case) or removed from the system (“2nd order” case), depending on whether the local ground state of  $H_{2,3}$  has a degeneracy of  $2\tilde{S} + 1$  or is a non-degenerate singlet, respectively. The set of renormalized couplings  $\tilde{\mathbf{K}} = (\tilde{K}^{(1)}, \dots, \tilde{K}^{(J_{\max})})$  are given by Eqs. (18) and (25), respectively.

of freedom interacts with the nearest-neighbor spins via the renormalized couplings given by Eq. (18). Upon decimation, the coupling constants and the spins change. For a complete description of the RG flow, one then needs to keep track of the joint distribution of coupling constants and spin sizes at the cutoff energy scale  $\Omega$ :  $\mathcal{Q}(\tilde{\mathbf{K}}, \tilde{S}; \Omega)$ , where  $\tilde{\mathbf{K}} = (K^{(1)}, \dots, K^{(J_{\max})})$ . The distribution of a particular variable can be obtained by integrating out the other ones. For instance, the distribution of the  $I$ -th coupling is  $\mathcal{P}_I(K; \Omega) = \sum_S \int \prod_{J \neq I} dK^{(J)} \mathcal{Q}(\tilde{\mathbf{K}}, \tilde{S}; \Omega)$ . In what follows, we analyze the fixed points of our SDRG flow.

#### IV. TECHNICAL SUMMARY OF THE RG FLOW AND THE CORRESPONDING ZERO-TEMPERATURE PHASES

Given the prescriptions of the strong-disorder renormalization-group method derived in Sec. III, we are now set to apply the SDRG decimation procedure to our system Hamiltonian (9) and analyze the general features of the RG flow. A complete characterization involves (i) finding all the fixed points, (ii) classifying their stability, and (iii) determining their basins of attraction in the case of totally attractive fixed points. The fixed points are characterized by the joint distribution of spin sizes and the  $J_{\max}$  coupling constants  $\mathcal{Q}^*(\mathbf{K}, S)$  (we denote a fixed-point distribution by the superscript  $*$ ). Accomplishing these three tasks allows us to determine the phase diagram of the system and the low-energy physical behavior. As one can guess, this is not an easy task and simplifications are needed. Below, we give a summary of the structure of the RG flow and the simplifications that can be made after one knows the fixed point distributions. We will focus on the fully stable fixed points, which determine the stable phases of the system.

One way of thinking about the problem is the fol-

lowing. Consider the set of vectors  $\{\omega_i\}$  where  $\omega_i = (S_i, \mathbf{K}_i, S_{i+1})$  and  $\mathbf{K}_i = (K_i^{(1)}, \dots, K_i^{(J_{\max})})$  is the vector of coupling constants. The set  $\{\omega_i\}$  defines the Hamiltonian (9). In the RG framework, it defines an initial condition of the RG flow. In the  $\mathbb{R}^{J_{\max}+2}$  space, this initial condition is just a set of vectors sharing the same origin. Under the RG flow, these vectors change their lengths and directions until they converge to a fixed-point distribution, which can be viewed as another set of vectors  $\{\omega_i^*\}$ . We have carried out this detailed analysis and found the possible fixed-point distributions of this system. As will be shown latter, the fully stable fixed point distributions can be classified in two major groups: one that has essentially AF correlations (but without AF long range order) and another characterized by strong FM tendencies. We now discuss their generic features.

The group of AF stable fixed points is characterized by a single spin size,  $\mathcal{Q}^*(\mathbf{K}_i, S_i) = \mathcal{R}^*(\mathbf{K}_i) \delta_{S, S_i}$ . Furthermore, the distribution of coupling constants is such that its support lies strictly along a single coordinate axis  $I$  in the  $J_{\max}$ -dimensional space of vectors  $\mathbf{K}_i$ ,  $K_i^{(J)} = K_i^{(I)} \delta_{J, I}$ . In other words,

$$\mathcal{R}^*(\mathbf{K}_i) = \delta[K_i^{(1)}] \dots \delta[K_i^{(I-1)}] \mathcal{P}^*[K_i^{(I)}] \times \delta[K_i^{(I+1)}] \dots \delta[K_i^{(J_{\max})}]. \quad (26)$$

There are two possibilities for the distribution function  $\mathcal{P}^*(x)$ . In one case,  $K_i^{(I)}$  is strictly positive and

$$\mathcal{P}^*(x) = \theta(x) \frac{\psi^{-1} - 1}{\Omega \ln \Omega} \left(\frac{\Omega}{x}\right)^{1 - \frac{\psi^{-1} - 1}{\ln \Omega}}, \quad (27)$$

with  $\psi = 1/2$  being a universal tunneling exponent. The distribution in Eq. (27) represents an infinite-randomness fixed point, since its relative width (the ratio of its standard deviation to its average value) grows without bounds as  $\Omega \rightarrow 0$ . This form is familiar from the well-studied case of disordered AF Heisenberg chains<sup>4-6</sup>. The relation between energy  $\Omega$  and length  $L$  scales is activated, i.e.,  $\ln \Omega \sim -L^\psi$ . This has implications to many low-energy thermodynamic observables such magnetic susceptibility  $\chi \sim T^{-1} |\ln T|^{-1/\psi}$  and specific heat  $C \sim |\ln T|^{-1/\psi}$ . Moreover, they are associated with an emergent  $SU(2S+1)$  symmetry. Note that the form of the distribution in this case varies as the cutoff  $\Omega$  is reduced. It can be regarded as describing a *fixed* point, however, if one rescales the variables appropriately by the cutoff:<sup>4</sup> if  $\zeta = \ln(\Omega/x)$  and  $\Gamma = \ln(\Omega_0/\Omega)$  (where  $\Omega_0$  is the initial value of the cutoff), then the  $\zeta$  distribution has the form  $\tilde{\mathcal{P}}^*(\zeta) = q^*(\zeta/\Gamma)/\Gamma$ , where  $q^*(x) = e^{-x}$  is indeed fixed. Since the fixed point is uniquely specified by a semi-axis direction in  $\mathbf{K}_i$  space, it can be represented by a point on the surface of the unit  $d$ -dimensional hypersphere, where  $d = J_{\max} - 1$ .

In the case of the other AF fixed point, the coupling

constants along the axis direction are either positive or negative *with equal probability*. This can only happen for chains with integer  $S > 1/2$ . The fixed-point distribution is still given by Eq. (27) (with  $x \rightarrow |x|$ ) but with the important difference in the tunneling exponent:  $\psi = 1/3$ . The other physical properties have the same form as above but with  $\psi = 1/3$ . The value  $I = J_S \neq 1$  depends on the spin size  $S$ . For the case of spin  $S = 1$ ,  $J_S = 2$  and this fixed-point is associated with an emergent SU(3) symmetry<sup>11</sup>. For other spin sizes, the symmetry is only the bare SU(2) symmetry. Strictly speaking, this AF fixed point cannot be represented as a single point on the surface of the unit  $d$ -dimensional hypersphere, since the coupling constants can have either sign.

Finally, there are two stable fixed points with strong FM instabilities. The first one is the usual Heisenberg FM fixed point for which  $K_i^{(1)} < 0$  and  $K_i^{(J>1)} = 0$  for all sites  $i$ . This model has been studied before<sup>25–29</sup> and we will not consider it in this paper. The other fixed point is characterized by *finite* effective disorder and only Heisenberg coupling constants with *both* FM and AF signs are present, namely,  $K_i^{(1)} \neq 0$  (with both signs) and  $K_i^{(J>1)} = 0$  for all sites  $i$ . This fixed point was thoroughly studied in Ref. 21 and is related to the so-called Large Spin phase. For weak disorder, the system is governed by a universal finite-disorder fixed point. For stronger disorder, the system flows to a line of finite-disorder fixed points. In any case, the distributions of FM and AF couplings are power laws  $\mathcal{P}^*(x) \sim |x|^{z-1}$ , with a non-universal exponent  $z$  which depends on the disorder strength but does not depend on the cutoff  $\Omega$ . The spin size distribution is expected to be a half normal whose width increases as the energy scale  $\Omega$  is lowered.

## V. FIXED POINTS AND THEIR STABILITY

We now analyze in more detail the general features of the RG flow, find all the AF fixed points and classify their stability. Our first result is obtained straightforwardly. If initially  $K_i^{(I)} \neq 0$  and  $K_i^{(J \neq I)} = 0$  (with  $1 \leq I \leq J_{\max} = 2S + 1$ ), then all the  $K_i^{(J \neq I)}$  remain zero throughout the entire RG flow since the couplings of ISTs of a given rank never generate couplings of ISTs of other ranks [see Eqs. (18) and (25)]. Describing the stability and the corresponding fixed-point distribution of spin sizes and coupling constants is a task we accomplish in what follows.

### A. Pairwise random singlet states

For simplicity, let us start our discussion focusing on the simplest case: initially  $K_i^{(I)} \neq 0$ ,  $K_i^{(J \neq I)} = 0$ , and the ground state of the local Hamiltonian  $H_{2,3}$  (see Fig. 1) is always a singlet. If this is the case, every decimation

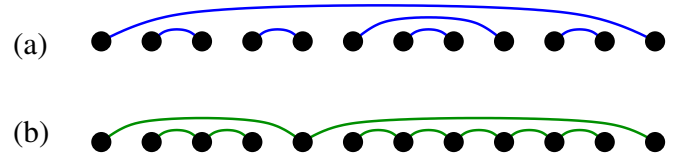


Figure 2. (Color online) A schematic depiction of two possible random singlet states. (a) A pairwise random singlet state in which each spin forms a singlet state with another spin indicated by the connecting line. (b) A triplewise random singlet state in which spin trios (connected by the lines) form a singlet state. Occasionally, a group of six (or other multiple of 3) spins can also form a singlet state. Most of the (pairs or trios of) singlets are formed by nearby spins, but there are also singlets formed by spins that are arbitrarily far apart from each other.

step involves second-order perturbation theory, as given by Eq. (25). The RG flow is well understood and is just like the one of the random AF spin-1/2 chain.<sup>4</sup> The spin size  $S$  remains fixed and the fixed-point coupling constant distribution  $\mathcal{P}^*(K^{(I)})$  is given by Eq. (27) with  $\psi = 1/2$ . This is an infinite-randomness fixed point since the relative width of the distribution increases without bonds at low energy scales, namely,  $\sigma_{K_I} / \langle K_I \rangle \rightarrow \infty$  as  $\Omega \rightarrow 0$ . This provides *a posteriori* justification of the perturbative RG treatment yielding asymptotically exact results. Its thermodynamics and the correlation functions can be computed straightforwardly. For a review, see Ref. 2. Moreover, the corresponding ground state is a collection of nearly independent singlets each of which is formed by only 2 spins [see Fig. 2(a)], hence the title of this subsection. We stress that, in principle, it is possible to form singlet states with 2 or more spins as depicted in Fig. 2(b). These will be relevant later.

Naturally, we must inquire about the conditions under which such a random singlet state is obtained, i.e., what are the values of spin size  $S$  and IST coupling rank  $I$  which ensure that the local ground state is always a 2-spin singlet. Although we could not obtain a rigorous analytical proof, our extensive numerical verification (see Appendix E) indicates that such singlet state is the ground state of  $H_{i,i+1}$  [see Eq. (9)] whenever  $K_i^{(J \neq I)} = 0$  and  $(-1)^I K_i^{(I)} < 0$  for any spin value  $S_i = S_{i+1} = S$ . Moreover, the sign of the renormalized  $\tilde{K}_i^{(I)}$  is a constant of the flow (see App. B), which is a necessary condition to ensure that all decimations will be of singlet-formation type (“second-order” case in Fig. 1).

Finally, we are now able to completely describe our first set of fixed points. It has the following features: (i) all spins have the same size  $S_i = S$ ; (ii) all the coupling constants are zero except for the ones corresponding to ISTs of rank  $I$ , and all of the latter have the same sign, equal to  $(-1)^{I+1}$ ; (iii) the fixed-point distribution of non-zero couplings is  $\mathcal{P}^*(x)$  as given by Eq. (27) with  $\psi = 1/2$  and  $0 < x = (-1)^{I+1} K^{(I)} < \Omega$ . There is a caveat, though. The cutoff energy scale  $\Omega$  is defined as the maximum

value of the local gaps. As the local gap is proportional to  $K_i^{(J)}$ , the corresponding numerical pre-factor can be absorbed in the definition of  $x$ .

Having found this set of  $J_{\max}$  fixed points of infinite-randomness type, the natural questions that arise are whether they are stable or not and what is the size of their basins of attraction. We now discuss their stability properties. The other question will be dealt with in Secs. VI and VII.

For each fixed-point of rank  $I$ , there are  $J_{\max} - 1$  independent perpendicular directions. Let us call  $\delta_i^{(J)}$  the relative deviation from the  $I$ -th axis in the  $J$ -direction with  $J \neq I$  at site  $i$ , namely,  $\delta_i^{(J)} = \frac{K_i^{(J)} - K_i^{(J)*}}{K_i^{(I)}}$ , where  $K_i^{(J)*} = 0$  is the fixed-point value. To leading order in  $\delta^{(J)}$ , the recursion relations (25) become

$$\tilde{\delta}_{1,4}^{(J)} \propto \delta_1^{(J)} \delta_3^{(J)}, \quad (28)$$

where the numerical pre-factor (whose magnitude is of order unity) is irrelevant for our purposes. Following the steps of Ref. 4, it is easy to show that the mean value of  $\ln |\tilde{\delta}_i^{(J)}|$  goes as  $\sim -c\Gamma^\phi$ , where  $c$  is a non-universal constant and  $\phi = \frac{1+\sqrt{5}}{2}$  is the golden mean, which implies a vanishing typical value  $\tilde{\delta}_{typ}^{(J)} \sim \exp(-c\Gamma^\phi)$ . Thus, weak deviations in any of the perpendicular directions are strongly irrelevant and all the  $J_{\max}$  fixed points mentioned above are stable.

We now search for other fixed points. Let us keep focusing on fixed points for which the only possible decimations are of the 2-spin singlet-formation variety. It is useful to rewrite the transformation rule (25) in terms of ratios of coupling constants, “angular variables” in the unit hypersphere in  $\mathbf{K}$  space. For concreteness, let us consider the case where  $K_i^{(1)}$  is non-zero and define  $s_i^{(J)} = \frac{K_i^{(J)}}{K_i^{(1)}}$ , ( $2 \leq J \leq J_{\max}$ ). The generalization to the other cases is straightforward. The recursion relations (25) can be rewritten as

$$\tilde{K}_{1,4}^{(1)} = \Sigma^{(1)}(S, \mathbf{s}_2) \frac{K_1^{(1)} K_3^{(1)}}{K_2^{(1)}}. \quad (29)$$

$$\tilde{s}_{1,4}^{(J)} = \Xi^{(J)}(S, \mathbf{s}_2) s_1^{(J)} s_3^{(J)}, \quad (J = 2, \dots, J_{\max}) \quad (30)$$

where  $S = S_2 = S_3$  is the spin size,  $\Sigma^{(J)}(S, \mathbf{s}_2) = 2 \frac{g(J, S)}{\Delta E(0, J)} K_2^{(1)}$ ,  $\mathbf{s}_i = \{s_i^{(2)}, \dots, s_i^{(J_{\max})}\}$  denotes the set of  $J_{\max} - 1$  angular variables, and  $\Xi^{(J)}(S, \mathbf{s}_2) = \Sigma^{(J)}(S, \mathbf{s}_2) / \Sigma^{(1)}(S, \mathbf{s}_2)$ . Note that the local energy scale at site 2 is essentially given by  $K_2^{(1)}$ . Thus, the functions  $\Sigma^{(1)}(S, \mathbf{s}_2)$  and  $\Xi^{(J)}(S, \mathbf{s}_2)$  are just geometric functions which are independent of  $K_2^{(1)}$ . This separation between the energy variable  $K^{(1)}$  and the set  $\mathbf{s}_2$  is what allows us to find the conditions under which  $\tilde{s}$  is kept constant

under the RG flow.

At a FP, the set  $\mathbf{s}_i$  becomes site-independent. Denoting its fixed point value by  $\mathbf{s}^*$ , then

$$s^{(J)*} = \Xi^{(J)}(S, \mathbf{s}^*) s^{(J)*} s^{(J)*}. \quad (31)$$

Thus, if  $s^{(J)*} \neq 0$ , we must have  $\Xi^{(J)}(S, \mathbf{s}^*) s^{(J)*} = 1$ . Solving the  $J_{\max} - 1$  coupled Eqs. (31) gives us all the FPs corresponding to the usual random 2-spin singlet states. Since the geometric prefactor  $\Xi^{(J)}(S, \mathbf{s}^*)$  depends non-trivially on  $S$  and  $\mathbf{s}^*$ , we will have to solve Eqs. (31) on a case by case basis. This is done for  $S = 3/2$  in Section VI and  $S = 2$  in Appendix C. Here, we will assume that such fixed points are known and provide general stability criteria for them.

Defining  $\delta^{(J)} = s^{(J)} - s^{(J)*}$  and expanding Eq. (30) up to quadratic order in  $\delta$ , we obtain

$$\begin{aligned} \tilde{\delta}_{1,4}^{(J)} &= s^{(J)*} \Xi^{(J)*} \left( \delta_1^{(J)} + \delta_3^{(J)} \right) + s^{(J)*} \sum_{K=2}^{J_{\max}} \gamma^{(K)*} \delta_2^{(K)} \\ &\quad + \Xi^{(J)*} \delta_1^{(J)} \delta_3^{(J)}, \end{aligned} \quad (32)$$

where  $\Xi^{(J)*} = \Xi^{(J)}(S, \mathbf{s}^*)$  and  $\gamma^{(K)*} = \left. \frac{\partial \Xi^{(J)}}{\partial s_2^{(K)}} \right|_{\mathbf{s}_2 = \mathbf{s}^*}$ . Using  $\Xi^{(J)*} s^{(J)*} = 1$  for  $s^{(J)*} \neq 0$ , and keeping only the leading-order terms, we rewrite Eq. (32) as

$$\tilde{\delta}_{1,4}^{(J)} = \begin{cases} \delta_1^{(J)} + \delta_3^{(J)} + s^{(J)*} \sum_{K=2}^{J_{\max}} \gamma^{(K)*} \delta_2^{(K)}, & \text{if } s^{(J)*} \neq 0, \\ \Xi^{(J)*} \delta_1^{(J)} \delta_3^{(J)}, & \text{otherwise.} \end{cases} \quad (33)$$

Therefore, for  $s^{(J)*} \neq 0$ , the iterations of  $\delta^{(J)}$  correspond to a random walk and this quantity grows without bounds. More precisely, the typical value  $|\tilde{\delta}_{typ}^{(J)}| \sim \delta_0 \Gamma^{\alpha_{\text{asym}}} + \sigma_{0,\delta} \Gamma^{\alpha_{\text{sym}}}$ , with  $\alpha_{\text{asym}} = \frac{1}{2} \left( 1 + \sqrt{5 + 4 s^{(J)*} \gamma^{(J)*}} \right)$  and  $\alpha_{\text{sym}} = \frac{1}{4} \left( 1 + \sqrt{5 + 4 (s^{(J)*} \gamma^{(J)*})^2} \right)$ , where  $\delta_0$  and  $\sigma_{0,\delta}$  are the mean and the width of the bare distribution of  $\delta^{(J)}$ .<sup>4</sup> This means that perturbations in both the positive and the negative  $J$ -th directions are relevant. On the other hand if  $s^{(J)*} = 0$ , then (33) becomes identical to (28) and the typical value of  $|\delta^{(J)}| \sim \exp(-c\Gamma^\phi)$ , meaning the perturbations in both the negative and positive  $J$ -th direction are irrelevant.

We are now able to state a clear criterion for the stability of the 2-spin-singlet fixed points reported here. Let such a fixed point be located at  $\mathbf{s}^*$ , which defines a point on the surface of our unit hypersphere in  $\mathbb{R}^{J_{\max}}$ . Recall we are assuming  $K_i^{(1)} \neq 0$  and thus  $\mathbf{s}^* = 0$  means the fixed point is on the first cartesian axis in  $\mathbf{K}$  space. Then, the fixed point  $\mathbf{s}^*$  is stable with respect to any  $\text{SU}(2)$ -symmetric local perturbation in the  $\pm J$ -th directions pro-



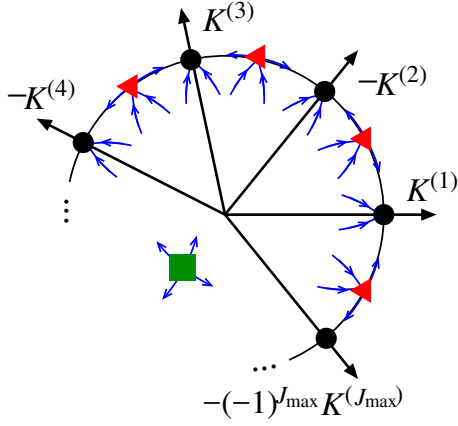


Figure 3. (Color online) Schematic drawing of the hyper-octant formed by all the fully stable AF fixed points of pairwise singlet nature [black circles on the  $(-1)^{J+1} K^{(J)}$  semi-axes]. Semi-stable AF fixed points exist on the hyperplanes formed by two (red triangles) or more (not shown) coordinate axis directions. There is also a totally unstable fixed point (green square) somewhere in the middle of the hyper-octant. This totally unstable fixed point is exactly  $SU(2S+1)$  symmetric while the other ones have emergent  $SU(2S+1)$  symmetry.

vided  $s^{(J)*} = 0$ ; otherwise, it is unstable in that direction. This is depicted schematically in Fig. 3 where we try to mimic a hyper-octant formed by the directions of the stable AF fixed points reported here. The stable fixed points are drawn as black circles. Fixed points which lie on coordinate hyper-planes (such as the  $K^{(1)} \times -K^{(2)}$  one) have both stable (out of the hyper-plane) and unstable (in hyper-plane) directions. These are drawn as red triangles. We will call them *planar fixed points*. Finally, a totally unstable fixed point (drawn as a green square) lies somewhere inside the hyper-octant.

Our first result is already very significant: the large number of completely stable AF fixed points along each coordinate axis in  $\mathbf{K}$  space define a hyper-octant on the surface of the unit hypersphere in  $\mathbb{R}^{J_{\max}}$  in which only pairwise singlet-formation decimations takes place (the 2nd-order route in Fig. 1). Therefore, all of these fixed-points (including the unstable ones inside the hyper-octant), despite being different, are characterized by a unique pairwise random singlet state [see Fig. 2(a)]. As will be shown in detail for the cases of  $S = 3/2$  and  $S = 2$  in Secs. VI and VII, respectively, they all exhibit an *emergent*  $SU(N)$  symmetry with  $N = 2S + 1$ , as reported before for the particular case of spin-1 systems.<sup>11</sup> Indeed (see Appendix D), the completely unstable fixed point in the middle of this hyper-octant is *exactly*  $SU(N)$ -symmetric, i.e., at that particular point, the  $SU(2)$  symmetric Hamiltonian (1) can be recast as a random AF Heisenberg  $SU(N)$  chain where the “spin” operators at odd (even) sites are generators of the fundamental (anti-fundamental) representation of the  $SU(N)$  group.

Recently,<sup>11</sup> we have shown that  $SU(2)$ -symmetric

random spin-1 chains realize distinct random singlet phases with emergent  $SU(3)$  symmetry, which we called “mesonic” and “baryonic”. Our first result shows that the pairwise random singlet state of the usual spin- $S$  random Heisenberg chain displays emergent  $SU(2S+1)$  symmetry. This ground state is the same in all other fixed points inside the AF hyper-octant of Fig. 3. Therefore, we can conclude that the totally unstable fixed point in the middle of this hyper-octant, which is exactly  $SU(2S+1)$  symmetric, governs the low-energy physics of entire hyper-octant. In this sense, the hyper-octant is the region in parameter space where deformations of the  $SU(2S+1)$  symmetric FP does not destroy the  $SU(2S+1)$  symmetry of the ground state of the local Hamiltonian  $H_{i,i+1}$ . Furthermore, we can view all the pairwise random singlet states as a generalization to higher spins of the “mesonic” random singlet state found in the spin-1 case,<sup>11</sup> in which the singlets are formed by a “particle”—“anti-particle” pair, corresponding to the fundamental and the anti-fundamental representations of  $SU(2S+1)$ .

### B. Triplewise random singlet states

We know that  $K_i^{(I)} \neq 0$  and  $K_i^{(J \neq I)} = 0$  is a fixed point of the RG flow but, so far, we have only explored the semi-axes with  $(-1)^I K_i^{(I)} < 0$  which define the AF hyper-octant of Fig. 3. What are the corresponding fixed points when we have the opposite signs  $(-1)^I K_i^{(I)} > 0$ , or when the signs are mixed? In general, since there will be no obvious singlet formation, the spin sizes will tend to increase and the flow becomes much more involved, a point we deal with later on. Here, however, we focus on a peculiar fixed point in which the spin size does not grow either, but instead remains fixed throughout the chain. How can this be possible? It is possible if the following requirement is fulfilled: whenever there is a decimation of “1st-order” type (see Fig. 1), then the new renormalized spin size  $\tilde{S}$  must equal  $S$ . Hence, under the two conditions that (i)  $\tilde{S} = S$  and (ii) that all the couplings are of the same rank, i.e.,  $K_i^{(I)} \neq 0$  and  $K_i^{(J \neq I)} = 0$ , a different AF fixed point is realized.

We now inquire whether there are rank values  $I$  that satisfy the first requirement that  $\tilde{S} = S$ . Evidently,  $S$  is necessarily integer, as it must appear as the sum of two equal spins  $S$ . We have explicitly verified up to  $S = 9$  that there is always one and only one rank value  $I_S$  that fulfills this requirement, namely,  $I_1 = 2$  and  $I_S = 3$  for  $S = 2, \dots, 8$ . For  $S > 9$ , there is no  $I_S$  with  $\tilde{S} = S$  as a ground state. Therefore, the fixed point here reported only appears for integer spins  $S \leq 8$ .

Let us now discuss the corresponding fixed-point distribution. Suppose that only 1st-order decimations occur. This necessarily requires that  $(-1)^{I_S} K_i^{(I_S)} > 0$  for all  $i$  along the RG flow. For all of the rank values  $I_S$  we have found, however, the signs of the renormalized couplings  $\tilde{K}_i^{(I_S)}$  are reversed after “1st-order”-type renormaliza-

tions. Therefore, we conclude that this new fixed-point has coupling constants  $K_i^{(I_S)}$  with mixed signs. The fractions of positive and negative values can be obtained straightforwardly. Since a 1st-order decimation always reverses the sign of the renormalized coupling constant, it favors equal fractions of positive and negative signs. As these fractions are preserved by 2nd-order decimations [see Eq. (25)], we then conclude that there is an equal fraction of 1st-order and 2nd-order decimation steps at this fixed point. As shown in Ref. 9, this leads to an infinite-randomness fixed-point distribution  $\mathcal{P}^*(|K^{(I_S)}|)$  given by Eq. (27) but with a different universal tunneling exponent  $\psi = \frac{1}{3}$ . Furthermore, due to the 1st-order decimation steps, the singlets are not formed by spin pairs, but rather acquire a more complex structure which depends on the distribution of couplings constant signs. If in the bare Hamiltonian all the couplings are such that  $(-1)^{I_S} K_i^{(I_S)} > 0$ , then all the singlets formed have a number of spins that is a multiple of three as depicted in Fig. 2(b). If on the other hand the signs of the bare couplings are random, then the singlets can be formed by any number of spins. In any case, the probability of finding a singlet formed by  $m$  spins decays  $\sim m^{-x}$ , with  $x \approx 3.8$ , as we verified numerically.

For the case of the spin-1 chain, it was shown that the corresponding triplewise random singlet state possesses an emergent SU(3) symmetry.<sup>11</sup> The difference with respect to the spin-1 pairwise random singlet state, which also possesses SU(3) symmetry, is the representation of the spin operators. While in the latter case the spin operators on odd (even) sites are the generators of the fundamental (anti-fundamental) representation of the SU(3) group, in the former case they are all generators of the fundamental representation. In the general case of spin- $S$  chains, however, this triplewise random singlet state does not possess an obvious enlarged symmetry.

Finally, we report that this peculiar AF fixed point is also stable against small SU(2) perturbations along the other transverse directions. This can be shown by a similar analysis as was done for the previous case of pairwise random singlet states. The analysis, however, is more involved due to the presence of 1st-order decimation steps as well. In addition, we have verified it numerically for the cases of  $S = 1$  (see Ref. 11) and  $S = 2$  (see Sec. VII).

### C. Large Spin phase

In Sec. VA we have considered fixed points in which all the coupling constants have the same sign. In Sec. VB, we have considered the case in which both signs are present in the fixed-point Hamiltonian. For the latter case, however, a particular rank value  $I_S$  is required. In both cases, the spin size  $S$  remained constant. We now consider another particular case, namely, the case of the Heisenberg chain, i.e.,  $K_i^{(1)} \neq 0$  and  $K_i^{(I>1)} = 0$ .

The first case we discuss is the Heisenberg chain with

both AF and FM couplings. This is a very important special case because, as we will see, it has a large basin of attraction. This fixed point was thoroughly studied in Ref. 21 and we now summarize some of what is known. The fixed-point distribution of local gaps  $\Delta_i$  obeys the following scaling

$$\mathcal{Q}_1^*(\Delta, S) = \frac{x \mathcal{Q}_{\text{AF}}\left(\frac{\Delta}{\Omega}, \frac{S}{\Omega^\alpha}\right) + (1-x) \mathcal{Q}_{\text{FM}}\left(\frac{\Delta}{\Omega}, \frac{S}{\Omega^\alpha}\right)}{\Omega^{1+2\alpha}}, \quad (34)$$

where  $\alpha$  and  $x$  are constants. The latter is the fraction of AF couplings  $K_i^{(1)} > 0$ . In addition, it was shown that  $\mathcal{Q}_1^*$  is not of infinite-randomness type as in Eq. 27 but rather of a finite-disorder variety. As a consequence, the relation between energy and length scales is not activated but a more usual power law  $\Omega \sim L^{-z}$  where  $z = -1/(2\alpha) > 0$  is the critical dynamical exponent. The relation between  $\alpha$  and  $z$  comes from the fact that the average spin size grows as  $\langle S \rangle \sim \sqrt{L}$ , which can be viewed as a consequence of the decimations leading to a random walk in spin space. Because the effective spin increases without bounds, the corresponding phase is called a Large Spin Phase. Although the thermodynamics is relatively well understood (the magnetic susceptibility is Curie like  $\chi \sim T^{-1}$  and the specific heat vanishes as  $C \sim T^{1/z} |\ln T|$ ), the ground-state spin-spin correlations are not so.<sup>30</sup>

The fact that  $\alpha < 0$  implies that the width of the spin size distribution grows without bounds along the RG flow and, therefore, the fraction of 2nd-order decimations vanishes, since it requires an AF coupling shared by spins of the same size. Without the multiplicative structure of the 2nd-order decimation (notice that the length scales always renormalize additively), the scaling is no longer activated and the effective disorder does not grow indefinitely. Hence, a finite-disorder fixed point.

Finally, it was also found that there is a universal finite-disorder fixed point (with  $\alpha \approx -0.22$  and  $x \approx 0.63$ ) which attracts all systems whose bare disorder is below a critical value. Systems whose the bare disorder is greater than this critical value are attracted by a line of finite-disorder fixed points where the corresponding critical exponents are non-universal.

### D. Higher symmetry fixed points

So far, we have described: (i) the fixed points of the AF hyper-octant (see Sec. VA) which involve coupling constants with uniform signs  $(-1)^J K_i^{(J)} < 0$ ; the stable fixed points lie on the hyper-octant coordinate semi-axes while all the remaining ones are unstable fixed points; (ii) the stable AF fixed point in which the coupling constant sign is random and along the axis with rank  $I_S$  (see Sec. VB); (iii) the stable fixed point where the couplings belong to the first rank  $J = 1$  and also have random signs, which was extensively studied before<sup>21</sup> (see Sec. VC). We now list some other fixed points that have higher sym-

metry than  $SU(2)$  and discuss their implications on the RG flow.

It is always possible to fine-tune the IST couplings in order to realize a higher  $SU(2S+1)$  symmetry in the bare Hamiltonian (9). In Appendix D we show how to construct these Hamiltonians. In this case, we can rewrite the  $SU(2)$ -symmetric Hamiltonian as a Heisenberg chain of  $SU(2S+1)$  spins which are nothing but irreducible representations of the  $SU(2S+1)$  group. One of these higher-symmetric fixed points is the unstable one in the middle of the AF hyper-octant. Here, the higher-symmetric spins on even (odd) sites are generators of the fundamental (anti-fundamental) representation of the  $SU(2S+1)$  group. As we have discussed in Sec. V A, our SDRG method is well suited for treating this case.

Another case is the one in which all the higher-symmetric spins are generators of the fundamental irreducible representation of the  $SU(2S+1)$  group. Here, our SDRG method only works for the  $S = 1$  case.<sup>11</sup> The reason is very simple. Consider for instance the  $S = 2$  case. The Clebsch-Gordan series of the product of two fundamental irreducible representations of the  $SU(2)$  group, with  $N = 2S + 1 = 5$ , is  $5 \otimes 5 = 10 \oplus 15$ . Applying our SDRG method in the AF case, we then have to keep the 10-fold degenerate manifold. How such a degenerate manifold can be recast as an  $SU(2)$  spin of our Hamiltonian (9)? We need to match the local dimensions  $2\tilde{S} + 1 = 10$ . But the Clebsch-Gordan series of the product of two  $S = 2$   $SU(2)$  spins is  $5 \otimes 5 = 1 \oplus 3 \oplus 5 \oplus 7 \oplus 9$ . The only way to obtain the 10-fold degenerate manifold of the  $SU(5)$  case is by fine-tuning to degeneracy either the  $\tilde{S} = 0$  and  $\tilde{S} = 4$  multiplets or the  $\tilde{S} = 1$  and  $\tilde{S} = 3$  multiplets. In either case, we cannot use the SDRG idea of replacing both spins  $S_2$  and  $S_3$  by a single effective spin  $\tilde{S}$  as depicted in Fig. 1. In this case, one needs to replace  $S_2$  and  $S_3$  by two other spins. Furthermore, one will need to introduce new operators in order to keep the structure of the low-energy spectrum. The SDRG method then becomes considerably more involved and we will not deal with these complications in the present study. Instead, we point out that a generalization of the SDRG method to  $SU(N)$  symmetry is capable of handling this special case, as was done in Ref. 9.

Are there other higher-symmetric fixed points? Certainly there are as, for instance, exemplified by the FM counterpart of the two cases mentioned above. But we will not concern ourselves with them because of their instability against  $SU(2)$ -symmetric perturbations. Thus, they have little consequence for the determination of the phases of our model Hamiltonian (1). Naturally, they may govern the low-energy physics at phase transitions but the study of these is out of the scope of the present paper. For the cases of AF  $SU(N)$ -symmetric fixed points, nonetheless, the low-energy behavior is known.<sup>9</sup>

### E. Unknown fixed points: breakdown of perturbation theory?

As already pointed out, there are fixed points whenever the coupling vectors  $\mathbf{K}_i$  point in one of the rank directions. For the rank direction  $J = 1$ , our method recovers the one of Ref. 21 and we can completely characterize two possible fixed points: the AF infinite-randomness fixed point (see Sec. V A) for  $K_i^{(1)} > 0$  and  $S_i = S$  throughout the chain and the finite-disorder fixed point (see Sec. V C) in which the sign of  $K_i^{(1)}$  as well as the spin sizes  $S_i$  are random variables. For the special rank direction  $J = I_S$ , our method can also describe the corresponding fixed points as long as  $S_i = S$  in the bare Hamiltonian (see Sec. V B). Finally, for the cases in which  $S_i = S$  and  $(-1)^J K_i^{(J)} < 0$ , we also can describe the corresponding fixed point (see Sec. V A). Are there other fixed points?

We have studied the RG flow in all cases via a numerical implementation of the SDRG method (see Sec. III). In order to do so, we start with a chain of  $\sim 10^6$  spins with random  $K_i^{(J)}$  couplings, such that the ratios  $\frac{K_i^{(J)}}{K_i^{(1)}}$  are the same at all sites. In other words, our initial Hamiltonian has uniform initial angles and only radial disorder in  $\mathbf{K}$ -space. During the numerical flow, we follow the distributions of  $K_i^{(J)}$  and spin sizes, which allows us to fully characterize the RG flow numerically. We have found that there are a few cases in which the flow is “pathological” because all the renormalized couplings between sites vanish, as discussed in Sec. III 1. Note that, since the rank-1 renormalized coupling  $\tilde{K}_i^{(1)}$  never vanishes, a necessary condition for this “pathological” flow to occur is  $\tilde{K}_i^{(1)} = 0$  for all sites. It turns out that when this latter condition is met, then one or both of the routes for the appearance of vanishing coupling constants between sites is unavoidably generated along the RG flow. Once such a “special” bond is decimated, the corresponding renormalization leads to a broken chain. In those cases (see App. F), we have performed degenerate second-order perturbation theory and new operators are introduced. Nonetheless, we have found that upon further decimations, other zeroes appear requiring a treatment that goes to higher orders in perturbation theory. We have not pursued this further. Instead, we believe that other zeroes will appear and this is an intrinsic aspect of the problem. Within our theoretical framework, we are unable to decide whether these zeroes are the manifestation of the true low-energy physics of the problem or whether it is a simple artifact of the method, indicating its breakdown and pointing to fundamentally new physics in these cases. We then leave as an open question the true low-energy behavior of these fixed points.

Nevertheless, in general, there will always be couplings of  $J = 1$  rank (the Heisenberg term) in the bare Hamiltonian. In this case, we argue that the flow is in general towards the FM or AF fixed points with only  $J = 1$  couplings. Indeed, in this case, only couplings of rank

$J = 1$  will survive and the flow is naturally towards the Large-Spin-phase fixed point. Furthermore, even if we were to carry out the perturbation theory to higher orders, the corresponding renormalized couplings would be typically much weaker than the  $J = 1$  renormalized couplings (which are finite in first order of perturbation theory). Therefore, these couplings will become sub-leading and the flow is towards the Large-Spin-phase fixed point.

In Secs. (VI) and (VII), we explore in more detail the RG flow for the cases of the spin  $S = 3/2$  and  $S = 2$  chains.

## VI. SPIN- $\frac{3}{2}$ CHAIN

In this section we apply the SDRG method derived in Sec. III to study the strong-disorder limit of the  $SU(2)$ -symmetric random spin- $\frac{3}{2}$  chain. For concreteness, we study the Hamiltonian (9) in which  $S_i = \frac{3}{2}$  for all  $i$  and the coupling vectors

$$\begin{aligned} \mathbf{K}_i &= (K_i^{(1)}, K_i^{(2)}, K_i^{(3)}) \\ &= K_i (\sin \theta_i \cos \phi_i, \sin \theta_i \sin \phi_i, \cos \theta_i) \end{aligned} \quad (35)$$

are distributed in the following way. The magnitude of the couplings  $K_i$  is distributed according to

$$P_0(K) = \frac{1}{\Omega_0 D} \left( \frac{\Omega_0}{K} \right)^{1-\frac{1}{D}}, \quad (36)$$

with  $0 < K_i < \Omega_0$ . Here  $\Omega_0$  is a microscopic high-energy cutoff and  $D$  parameterizes the bare disorder strength. First, we consider the angles  $\theta_i = \theta$  and  $\phi_i = \phi$  to be uniform throughout the chain. Note that in this case the unit hyper-sphere is the 2-sphere in  $\mathbb{R}^3$ . We will thus determine the phase diagram on the surface of the 2-sphere. At the end of this section, we analyze the case of random initial angles.

### A. The antiferromagnetic octant

Particularizing the results of Sec. V A to the case  $S_i = 3/2$  we know that there must be  $J_{\max} = 2S = 3$  stable AF fixed points along the three coordinate semi-axes defined by  $K_i^{(1)} > 0$ ,  $K_i^{(2)} < 0$ , and  $K_i^{(3)} > 0$ . Furthermore, these semi-axes define an octant on the surface of the 2-sphere where only 2nd-order decimations occur since the ground state of the local Hamiltonian (9) is always a singlet [see Fig. 1]. In this case, the renormalized coupling constants are given by Eqs. (25), which we rewrite as

$$\tilde{K}^{(J)} = \frac{K_1^{(J)} K_3^{(J)}}{\mathbf{v}^{(J)} \cdot \mathbf{K}_2}, \quad (37)$$

with the vectors  $\mathbf{v}^{(1)} = \frac{1}{5}(2, -30, 147)$ ,  $\mathbf{v}^{(2)} = -\frac{1}{10}(4, -40, 49)$ , and  $\mathbf{v}^{(3)} = \frac{1}{35}(16, -40, 126)$ . We ex-

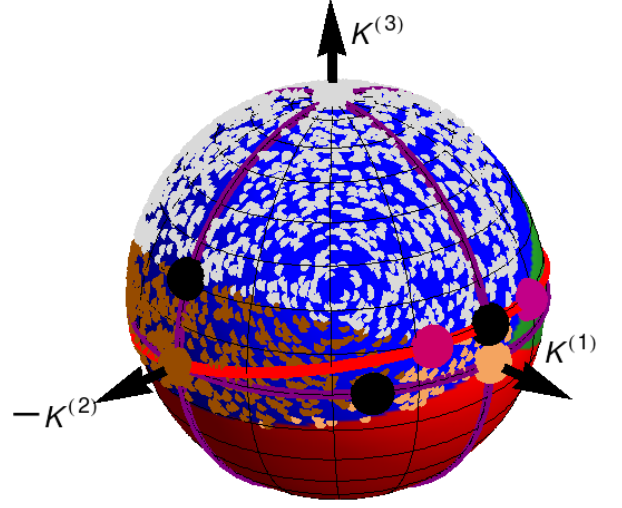


Figure 4. (Color online) Schematic phase diagram of the disordered spin- $\frac{3}{2}$  chain on and around the AF octant  $K^{(1)} \times -K^{(2)} \times K^{(3)}$ . The thick dots on the surface of the sphere represent initial conditions of the numerical RG flow. The dots are colored according to their fate in the flow and, therefore, map out the distinct basins of attraction. The beige dots flow to the  $K^{(1)} > 0$  (Heisenberg) fixed point (beige circle), the brown ones to the  $K^{(2)} < 0$  fixed point (brown circle), while the white ones have only  $K^{(3)} > 0$  couplings at the fixed-point Hamiltonian (white circle on the North pole). The pink fixed point in the middle of the octant is totally unstable and has an exact  $SU(4)$  symmetry. The other semi-stable fixed points are represented as black circles. The ground state of the *local* Hamiltonians [ $H_{23}$  in Eq. (13)] is indicated by the background color, see Table II for the color scheme (the FM  $\tilde{S} = 3$  orange region is not visible from this viewing angle). The red and green regions (not marked by any dot for clarity) correspond to the LSP fixed-point. On the red line, the system has an exact  $SO(5)$  symmetry.

plicitly verified these results by numerically implementing the SDRG decimations.

In Fig. 4 we plot the resulting flow diagram on and around the AF octant. We have chosen many initial conditions, parameterized by the initial angles  $\theta, \phi$  (represented as thick dots) and disorder strength  $D$ . We confirm the flow to be independent on  $D$  (as long as  $D$  is sufficiently large). For small  $D$ , one has to be careful. A consistent approach would be to treat the perturbations to the local Hamiltonian (13) to higher orders of perturbation theory than the second.<sup>31</sup> This approach becomes much more involved and we do not do it the present study. Nonetheless, it is worth mentioning that, even at the Heisenberg point this issue is still controversial. In this case, the recursion relation (37) reduces to  $\tilde{K}^{(1)} = \frac{5K_1^{(1)}K_3^{(1)}}{2K_2^{(1)}}$ . The numerical prefactor  $\frac{5}{2} > 1$ , which means the renormalized coupling can be bigger than the decimated ones if the bare disorder is weak. Therefore, the decimation procedure is internally inconsistent. As a result, it has been argued that the weak-



disorder regime corresponds to a random singlet state with spin-1/2 rather than 3/2 excitations<sup>32</sup>. Another view is that weak disorder is irrelevant<sup>33,34</sup>. In all of these studies, however, there is general agreement that at strong disorder the ground state is a spin-3/2 random singlet state as reported here.

The dots on the surface of the sphere are colored according to the corresponding fixed point to which they flow (beige, brown and white circles on the axes). As expected, all initial conditions inside the AF octant flow to one of the stable fixed points on the axes of the octant. Note that they attract even other initial conditions outside (but close to) the AF octant. The corresponding pairwise RSP has, therefore, a large basin of attraction. In addition, we display the semi-stable planar fixed points (black circles) as well as the totally unstable SU(4) symmetric fixed point (pink circle) inside the octant. Their locations are determined analytically, as shown below, and agree with our numerical data.

In order to find the location of the fixed points, we need to solve Eq. (31) for the  $S = 3/2$  case. Defining the vector  $\mathbf{s}_i = (s_i^{(2)}, s_i^{(3)})$  where  $s_i^{(2,3)} = \frac{K_i^{(2,3)}}{K_i^{(1)}}$ , then from Eq. (37) we have

$$\tilde{s}^{(2)} = -2s_1^{(2)} s_3^{(2)} \left( \frac{2 - 30s_2^{(2)} + 147s_2^{(3)}}{4 - 40s_2^{(2)} + 49s_2^{(3)}} \right), \quad (38)$$

$$\tilde{s}^{(3)} = \frac{7}{2}s_1^{(3)} s_3^{(3)} \left( \frac{2 - 30s_2^{(2)} + 147s_2^{(3)}}{8 - 20s_2^{(2)} + 63s_2^{(3)}} \right). \quad (39)$$

Since the fixed points are such that  $\mathbf{s}_i = \tilde{\mathbf{s}}_i = \mathbf{s}^*$ , we find the following physical solutions besides the three stable ones already obtained  $K_i^{(J)} = K_i \delta_{J,K}$ , with  $J = 1, 2, 3$ : (i) the semi-stable AF fixed point on the  $K^{(3)} = 0$  plane  $\mathbf{s}_4^* = -\frac{1}{30}(9 + \sqrt{141})(1, 0) \approx (-0.70, 0)$ , which corresponds to  $(\theta_4^*, \phi_4^*) \approx (\frac{\pi}{2}, -35^\circ)$ ; (ii) the semi-stable AF fixed point on the  $K^{(2)} = 0$  plane  $\mathbf{s}_5^* = (0, \frac{4}{21}) \approx (0, 0.19)$ , or  $(\theta_5^*, \phi_5^*) \approx (79^\circ, 0)$ ; (iii) the semi-stable AF fixed point on the  $K^{(1)} = 0$  plane at which  $|s_6^*|$  is infinite but  $s_6^{(3)*}/s_6^{(2)*} = \frac{2}{49}(1 - \sqrt{141}) \approx -0.44$  is finite; this is equivalent to  $(\theta_6^*, \phi_6^*) \approx (66^\circ, -\frac{\pi}{2})$ ; and (iv) the totally unstable SU(4)-symmetric fixed point  $\mathbf{s}_7^* = (-\frac{1}{3}, \frac{4}{21})$ , which corresponds to  $(\theta_7^*, \phi_7^*) \approx (80^\circ, -18^\circ)$ . Notice all these solutions obey the restriction  $(-1)^J K_i^{(J)*} \leq 0$ . Besides these seven solutions, there are additional ones [for instance  $(\frac{2}{3}, \frac{4}{21})$ ] which are, however, nonphysical since the singlet is not the ground state of the local Hamiltonian.

As anticipated in Section V A, we note that the unstable AF SU(4)-symmetric point can be adiabatically connected to *all* the other AF stable fixed points. In other words, the ground state *throughout the AF region* is a collection of the same singlets as at the SU(4) symmetric point. These singlets are, therefore, SU(4) singlets, and the ground state is SU(4) invariant. This is one of our main findings: the ground state singlets inherit the

symmetry of the SU(4) fixed points. The same is true of the lowest excitations, essentially free spins, which can be seen as transforming according to either the fundamental of the anti-fundamental representations of SU(4). The low-energy sector has, therefore, an emergent SU(4) symmetry, analogous to the mesonic SU(3) RSP found before in spin-1 systems.<sup>11</sup>

As for the other regions of the phase space, we find generically that the flow is towards a LSP, with only  $K_i^{(1)} \neq 0$ , except in the region where  $\tilde{S} = 3$  (not visible in Fig. 4), where the phase is ferromagnetic.

## B. SO(5) line and SU(4) points

As shown in Ref. 15, the Hamiltonian of isotropic spin- $\frac{3}{2}$  chains has an enlarged SO(5) symmetry in a certain region of parameter space. Even more interesting, this region happens to be the one accessible to cold-atom experiments. In such experiments, for spin- $\frac{3}{2}$  particles at quarter filling and in the limit of strong interactions, selection rules for the scattering of two atoms at low energies impose that only channels of even total angular momentum are allowed. In this case, putting  $\epsilon_i^{(1)} = \epsilon_i^{(3)} = 0$  in the Hamiltonian of Eq. (12) we get

$$H_{\text{SO}(5)} = \sum_{i=1}^{N_{\text{sites}}} \epsilon_i^{(0)} P_0(\mathbf{S}_i, \mathbf{S}_{i+1}) + \epsilon_i^{(2)} P_2(\mathbf{S}_i, \mathbf{S}_{i+1}), \quad (40)$$

which was shown to possess an exact SO(5) symmetry.<sup>15</sup> The IST coupling constants then are, neglecting a constant contribution (see Appendix A)

$$K_i^{(1)} = -\frac{\pi}{15} (\epsilon_i^{(0)} + \epsilon_i^{(2)}), \quad (41)$$

$$K_i^{(2)} = \frac{\pi}{45} (\epsilon_i^{(0)} - 3\epsilon_i^{(2)}), \quad (42)$$

$$K_i^{(3)} = -\frac{4\pi}{315} (\epsilon_i^{(0)} + \epsilon_i^{(2)}). \quad (43)$$

The vector  $\mathbf{s}_i = (K_i^{(2)}, K_i^{(3)})/K_i^{(1)} = (\varepsilon_i, \frac{4}{21})$ , where  $\varepsilon_i = [\epsilon_i^{(2)} - \epsilon_i^{(0)}/3] / [\epsilon_i^{(2)} + \epsilon_i^{(0)}]$ , with  $-\infty < \varepsilon_i < \infty$  a free parameter. Thus, the parameter space in which the SO(5) symmetry is realized is a line on the surface of our 2-sphere. This is shown as the red line in Fig. 4. Interestingly, this line contains three of the AF fixed points found:  $\mathbf{s}_2^* = (-\infty, x)$ , with  $x$  being any finite number (this corresponds to the totally stable fixed point  $K_i^{(2)} < 0$  and  $K_i^{(1)} = K_i^{(3)} = 0$ ),  $\mathbf{s}_5^*$  (the semi-stable fixed point on the  $K_i^{(2)} = 0$  plane) and  $\mathbf{s}_7^*$  [the totally unstable SU(4)-symmetric fixed point].

As shown in Appendix D (see also<sup>15,35</sup>), the Hamiltonian

$$H_{4-\bar{4}}^{\text{SU}(4)} = \sum_i K_i \left( \hat{O}_1 - \frac{1}{3} \hat{O}_2 + \frac{4}{21} \hat{O}_3 \right), \quad (44)$$

with generic  $K_i$ , which corresponds to  $\mathbf{s}_i = (-\frac{1}{3}, \frac{4}{21})$ , is SU(4)-symmetric. This is indeed the totally unstable fixed point  $\mathbf{s}_7^*$  in the AF case ( $K_i > 0$ ). The notation  $4 - \bar{4}$  indicates that the Hamiltonian (44) corresponds to a Heisenberg SU(4) spin chain with “spin” operators on odd (even) sites which are the generators of the fundamental (anti-fundamental) representation of the SU(4) group. In addition, there is another AF SU(4)-symmetric Hamiltonian given by

$$H_{4-\bar{4}}^{\text{SU}(4)} = \sum_i K_i \left( \hat{O}_1 + \frac{1}{3} \hat{O}_2 + \frac{4}{21} \hat{O}_3 \right). \quad (45)$$

The difference with respect to the Hamiltonian (44) is that all the “spin” operators are generators of the fundamental representation of the SU(4) group regardless of the lattice site. Although our SDRG scheme is not suitable for treating this case (since the multiplets  $\tilde{S} = 0$  and  $\tilde{S} = 2$  become degenerate in the ground state of the local Hamiltonian), we know this must be a fixed point of the RG, since it has to preserve the symmetry. We then denote this fixed point by  $\mathbf{s}_8^* = (\frac{1}{3}, \frac{4}{21})$ , which corresponds to  $(\theta_8^*, \phi_8^*) \approx (80^\circ, 18^\circ)$ , see the pink circle in Fig. 4. Indeed, in Ref. 9 it was shown that the low-energy physics of this SU(4)  $4 - \bar{4}$  Hamiltonian is governed by an infinite-randomness fixed point, with the local energy scales being distributed according to Eq. (27) with a universal tunneling exponent  $\psi = \frac{1}{4}$ . In addition, the corresponding ground state is a random singlet state whose singlets are formed by groups of spins which are multiples of 4: a 4-fold random singlet state analogous to the triplwise random singlet state depicted in Fig. 2(b).

Therefore, the SO(5) line contains both AF SU(4)-symmetric fixed points  $\mathbf{s}_7^*$  and  $\mathbf{s}_8^*$ . In addition, the fixed points  $\mathbf{s}_{2,5}^*$  are also exactly SO(5) symmetric. Nonetheless, recall they have an emergent SU(4) symmetry.

We have also verified that the SO(5) line is a constant of the flow. Let us explain this a little further. Starting from any point  $(\theta, \phi)$  on the surface of the 2-sphere in Fig. 4, the angles change along the RG flow in such a way that one cannot represent the renormalized Hamiltonian by a single point  $(\tilde{\theta}, \tilde{\phi})$ , but rather by a distribution of angles. Generically, this distribution has support on two-dimensional manifolds on the 2-sphere. If one starts at any point on the SO(5) line, however, all the renormalized angles  $(\tilde{\theta}_i, \tilde{\phi}_i)$  will remain in the SO(5) line (a one-dimensional manifold) along the RG flow. This means that our SDRG scheme preserves the symmetry, as it should.

It is interesting to see that the unstable fixed points on this line are the points with a larger SU(4) symmetry. Between them there is the semi-stable fixed point  $\mathbf{s}_5^*$ . As

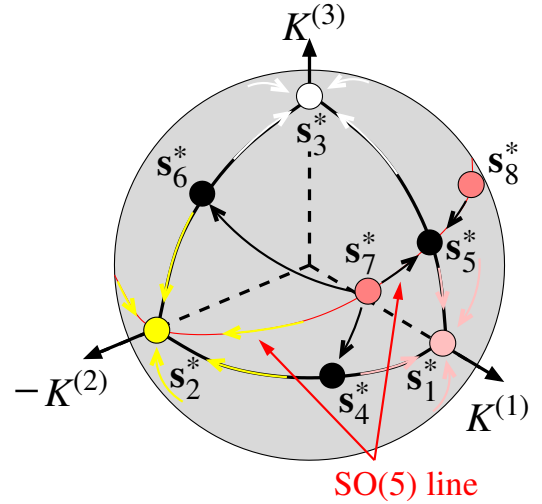


Figure 5. Schematic flow diagram of the *average* angular variables in the AF octant of random spin- $\frac{3}{2}$  chains (based on the phase diagram of Fig 4). See text for details about the fixed points  $\mathbf{s}_i^*$ .

we will see below, the SU(4)-symmetric  $4 - \bar{4}$  fixed point  $\mathbf{s}_8^*$  governs the transition between the AF phase and the Large Spin phase. The topology of the flow requires that there be another fixed point towards the southwest of the totally stable fixed point  $\mathbf{s}_2^*$ . Very likely, this fixed point delimits the transition between the FM and AF phases. Like in the spin-1 case,<sup>11</sup> this fixed point is a FM SU(4) symmetric fixed point.

It is visually instructive to follow the SDRG flow of the angular variables  $\mathbf{s}_i$ . It is useful to normalize them so the flow is confined to the surface of a unit sphere, as in Fig. 4. Several trajectories of the *average* values of  $\mathbf{s}_i$  are shown in Fig. 5. This gives some intuition about the way these variables approach the fixed points. We point out, however, that the flow of the *distribution* of  $\mathbf{s}_i$  is not captured by this figure. In particular, their widths start at zero, become non-zero at intermediate stages of the flow, and tend to zero again as the fixed points are approached.

### C. RG flow on the other semi-axes

As mentioned in Section III 1, the first-order perturbation theory steps yield a vanishing renormalized coupling constant in some special cases, even if the ground state multiplet is degenerate. Curiously, this happens for the spin-3/2 chain on the semi-axes  $K^{(2)} > 0$  and  $K^{(3)} < 0$ , i.e., on all other semi-axes except the ones of the AF octant and the purely FM Heisenberg axis  $K^{(1)} < 0$ . We show how to partially handle these cases, by finding the first non-zero contributions.

Before addressing the  $J > 1$  cases, let us start by reviewing the first rank case. If  $K_2^{(1)} < 0$ , the ground state is a spin  $\tilde{S} = 3$  and the RG rule is the one given in

Sec. VC. The mixing of random  $K_i^{(1)}$  signs leads to a LSP<sup>21</sup>, whereas exclusively negative couplings lead to a FM phase.

Now we focus on higher rank tensors. On the semi-axis  $K^{(2)} < 0$ , first-order perturbation theory generically gives (see Fig. 1 for a guide)

$$\tilde{K}_1^{(2)} = \frac{3\tilde{x}^2 + \tilde{x}(2x_2 - 6x_3 - 3) + 3(x_2 - x_3 - 1)(x_2 - x_3)}{2\tilde{x}(4\tilde{x} - 3)} \quad (46)$$

where  $x_i = S_i(S_i + 1)$  and  $\tilde{x} = \tilde{S}(\tilde{S} + 1)$ . The  $\tilde{K}_3^{(2)}$  renormalization follows analogously, by exchanging  $x_2 \rightleftharpoons x_3$ . Starting with a chain in which all spins are of size  $S_i = \frac{3}{2}$ , then already in the first decimation step  $x_2 = x_3 = \frac{15}{4}$ . As the ground state of the local Hamiltonian is  $\tilde{S} = 2$ , then first-order perturbation theory yields  $\tilde{K}_{1,3}^{(2)} = 0$ . In Appendix F, we have shown how to calculate second-order perturbative corrections. The steps are analogous to those shown in the second order calculations when the ground state is a singlet, except that the projector onto the ground state  $P_0$  has to be replaced by  $P_{\tilde{S}}$ . The net result, when three-body non-frustrating terms are neglected, is the appearance of a non-zero coupling between spin  $\mathbf{S}_1$  and the effective spin  $\tilde{\mathbf{S}}$

$$\Delta H_{1,2}^{(2)} = \frac{(K_1^{(2)})^2}{K_2^{(2)}} \left( \frac{9}{16} \hat{O}_1 - \frac{3}{56} \hat{O}_3 \right). \quad (47)$$

where  $\hat{O}_i = \hat{O}_i(\mathbf{S}_1 = \frac{3}{2}, \tilde{\mathbf{S}} = 2)$ . By symmetry, we obtain the coupling connecting the spin  $\tilde{\mathbf{S}}$  to site 4 by replacing  $1 \leftrightarrow 4$ . The RG rules are schematically shown in Fig. 10 of Appendix F. This prescription is enough to fix the first RG decimations, but the zeros proliferate again in later decimations. Up to the point at which the flow is not dominated by these zeros, we do not find indications of a Large Spin phase. The phase appears to be antiferromagnetic, even though its full characterization would require going to higher orders in perturbation theory.

Starting with a negative  $K_2^{(3)}$  gives us a spin  $\tilde{S} = 1$  as the ground state manifold. But a spin-1 Hamiltonian does not support third-rank ISTs (as a rule, remember that spin operators with  $2S < J$  do not form rank- $J$  ISTs). Note that this corresponds to case (a) discussed in Section III 1, whereas on the  $K^{(2)} < 0$  axis it was related to case (b) of that Section. In Appendix F, we show in detail how to compute second-order corrections for this case as well. The effective Hamiltonian that connects a spin  $S_1 = \frac{3}{2}$  with a spin  $\tilde{S} = 1$  is, neglecting three-body non-frustrating interactions, is

$$\Delta H_{1,2} = \frac{(K_1^{(3)})^2}{|K_2^{(3)}|} \left( \frac{63}{20} \hat{O}_1 + \frac{189}{100} \hat{O}_2 \right). \quad (48)$$

2-spin ground state	Color
$\tilde{S} = 0$	blue
$\tilde{S} = 1$	red
$\tilde{S} = 2$	green
$\tilde{S} = 3$	orange
$\tilde{S} = 4$	purple

Table II. Color scheme we are going to use for the identification of ground multiplets of the local Hamiltonian in the analysis of the spin- $\frac{3}{2}$  and spin-2 chains. The same applies to Figs. 4, 6, 8 and 9.

Here,  $\hat{O}_i = \hat{O}_i(\mathbf{S}_1 = \frac{3}{2}, \tilde{\mathbf{S}} = 1)$  and the analogous term for site 4 follows by symmetry. Again, this prescription is enough to fix only the first decimation steps. As before, there are no clear indications of a Large Spin phase being generated.

Clearly, further investigation is needed to characterize this phase. Either the inclusion of the three-body interactions remedy the vanishing renormalized interactions, or the proliferation of these zeroes are indeed part of the physics, indicating a breakdown of the perturbative treatment and that a new approach is necessary. We leave as an open question the elucidation of this problem. Here, we argue, however, that these problems have little effect on the generic RG flow. In general, the  $K_i^{(1)}$  couplings are nonzero and never yield any vanishing renormalizations. Therefore, they are dominant over the other higher-rank interactions and the generic RG flow will be towards the  $K_i^{(1)} \neq 0$  fixed points.

#### D. RG flow on planes

Having analyzed the behavior on the different semi-axes, we now explore planes on which two of the tensor couplings are non-zero. The 2-spin ground state structure is shown in Fig. 6. In Table II, we list the colors we are going to use to identify the ground multiplets in the study of both spin- $\frac{3}{2}$  and spin-2 chains.

The RG flow in the singlet (blue) region is towards the fully stable fixed points on the semi-axes discussed in Section VIA. We now address the flow in the other non-blue regions of the plane, where the ground state is not a singlet. We always assume the initial angles are uniform and the disorder is in the radial direction. Let us assume additionally that we do not start right on the axes, since these cases have been discussed previously.

Let us start by analyzing the  $K^{(1)} \times K^{(2)}$  and  $K^{(1)} \times K^{(3)}$  planes. In the orange region, the flow is towards the FM phase, with only  $K_i^{(1)} < 0$  remaining. Starting in both the red ( $\tilde{S} = 1$ ) or the green ( $\tilde{S} = 2$ ) regions, effective spins that are not equal to the original spin  $\frac{3}{2}$  are generated. Notice that, in both regions, only the  $K_i^{(1)} \neq 0$  couplings remain since the other ones are automatically

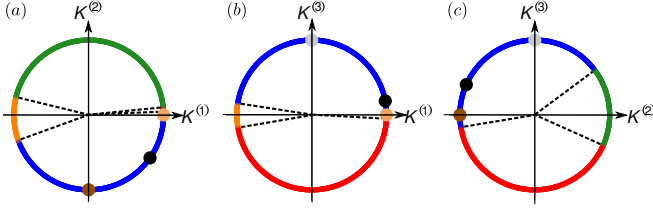


Figure 6. (Color online) Diagrams representing the 2-spin ground multiplet for two spins  $3/2$  and the AF RG fixed points of the disordered spin- $3/2$  chain. (a), (b) and (c) represent the  $K^{(3)} = 0$ ,  $K^{(2)} = 0$  and  $K^{(1)} = 0$  planes, respectively. The total angular momentum of the ground multiplets can be  $\tilde{S} = 0, 1, 2$  or  $3$ , which are identified by the color scheme of Table II. The small circles represent the AF angular fixed points. The stable AF ones lie on the semi-axes with  $K^{(1)} > 0$ ,  $K^{(2)} < 0$ , and  $K^{(3)} > 0$ . The unstable fixed points can also be found analytically (see the main text for details).

renormalized to zero, for the very same reasons discussed in the previous section. After some initial steps, we end up with a “soup” of spin  $\frac{3}{2}$  and spins  $\tilde{S}$  (equal to 2 or 1, depending on the case) coupled by  $K_i^{(1)}$  couplings. By numerically following the flow, we find out that after an initial transient, the spins start to grow and the flow is towards a LSP.

We now focus on the  $K^{(2)} \times K^{(3)}$  plane. In the green region of the first quadrant, the  $K_i^{(2)}$  couplings are renormalized to zero (due to the zeroes discussed in the previous section), effective spins  $\tilde{S} = 2$  are generated, and the corresponding renormalized couplings  $K_i^{(3)}$  are negative. The presence of both spins 2 and  $3/2$  gives rise to the RG rules shown in Table III (which can be found with the formulas derived in Section III and Appendix B). Interestingly, these rules are closed under the RG transformations. We find numerically that, at low energies, only rules of type 4 survive, and the phase is again a RSP on the  $K^{(3)} > 0$  semi-axes, with exponent  $\psi = \frac{1}{2}$ . Notice that, unlike the RSP found previously (in the blue region), this one depends strongly on the generated spins  $\tilde{S} \neq 0$  and the possible combinations of  $\tilde{S}$  and  $S = \frac{3}{2}$  on later RG steps. In the red region of the third quadrant, the RG flow is very similar to the one just discussed, with the changes  $K^{(2)} \rightleftharpoons -K^{(3)}$  and  $\tilde{S} = 1$ . Again, the low energy physics is found to be described by a RSP with exponent  $\psi = \frac{1}{2}$ , now on the  $K^{(2)} < 0$  semi-axis. In the fourth quadrant of this plane, the first RG decimations make one of the couplings, either  $K_i^{(2)}$  or  $K_i^{(3)}$ , vanish, depending on the region where the bond is located (red or green). At later RG steps, however, the remaining non-zero couplings also vanish. Therefore, we do not have the full low-energy description in this quadrant, as in the situation discussed in Section VIC. Note that a small perturbation in the perpendicular  $K^{(1)}$  direction already fixes this problem and drives the system towards a LSP.

## VII. SPIN-2 CHAIN

We now study the disordered spin-2 chain. The parameter space is spanned by  $J_{\max} = 4$  axes  $K_i^{(J)}$ , with  $J = 1, 2, 3, 4$ . The RG steps can be found in Appendix C. We will be brief on features that are analogous to the spin- $3/2$  case and will focus on the features which are new.

Let us start by focusing on the flow on the axes. As discussed before, the AF stable fixed points lie along the semi-axes  $K^{(1)} > 0$ ,  $K^{(2)} < 0$ ,  $K^{(3)} > 0$ , and  $K^{(4)} < 0$ . Each one of these cases leads to a pairwise RSP (see Section VA). This conclusion holds throughout the AF hyper-octant, in the unit 3-sphere, defined by the above four semi-axes. Like in the spin- $3/2$  case, the negative  $K^{(1)}$  semi-axis gives rise to a FM phase and to a LSP when  $K_i^{(1)}$  is both negative and positive. On the other semi-axes, with the exception of the negative  $K^{(3)}$  axis to be discussed later, our RG scheme suffers from the presence of zero renormalized couplings in first order of perturbation theory (see Sec. III 1), in close analogy to the spin- $3/2$  case (see Sec. VIC).

The  $K^{(3)}$  axis is special because it can also support a triplewise RSP as discussed in Sec. VB. Whenever  $K^{(3)} < 0$ , the corresponding first order decimation (see Fig. 1) yields an effective spin  $\tilde{S} = 2$ . Thus, the spin  $S = 2$  is a constant along the RG flow. In addition, the effective couplings  $\tilde{K}_{1,3}^{(3)}$  change signs meaning this new effective spin can be later second-order decimated with third spin into a singlet state. At the fixed point, the distribution of coupling constants is of the infinite-randomness type given by Eq. (27) with  $\psi = \frac{1}{3}$ . This universal fixed point attracts all initial conditions in which the  $K_i^{(3)}$  are either all negative or have mixed signs. Only in the case of positive signs  $K_i^{(3)} > 0$  for any  $i$  does the

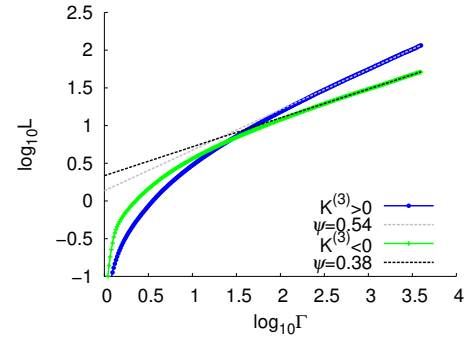


Figure 7. (Color online) Energy-length relation for couplings on the  $K^{(3)}$  axes, starting with all spins equal to  $S = 2$ . For negative initial values, the numerical value of the tunneling exponent is  $\psi \approx 0.38$ , while for positive initial values  $\psi = 0.54$ , compatible with the predicted values of  $\psi = \frac{1}{3}$  and  $\psi = \frac{1}{2}$ , respectively. We have decimated chains of size  $N_{\text{sites}} = 8 \times 10^6$ .



Rule	$S_2$	$S_3$	Couplings	$\tilde{S}$	RG rules
1	$\frac{3}{2}$	$\frac{3}{2}$	$K_2^{(2)} > 0, K_2^{(3)} > 0$	2	$\tilde{K}_{\{1,3\}}^{(3)} = -\frac{1}{4}K_{\{1,3\}}^{(3)}$ and $\tilde{K}_{\{1,3\}}^{(2)} = 0$
2	2	$\frac{3}{2}$	$K_2^{(3)} < 0, K_2^{(2)} = 0$	$\frac{3}{2}$	$\tilde{K}_1^{(3)} = -\frac{8}{5}K_1^{(3)}$ and $\tilde{K}_3^{(3)} = \frac{1}{5}K_3^{(3)}$
3	2	2	$K_2^{(3)} > 0, K_2^{(2)} = 0$	0	2nd order; $\tilde{K}_{1,3}^{(3)} = \frac{4}{9} \frac{K_1^{(3)} K_3^{(3)}}{K_2^{(3)}}$
4	$\frac{3}{2}$	$\frac{3}{2}$	$K_2^{(3)} > 0, K_2^{(2)} = 0$	0	2nd order; $\tilde{K}_{1,3}^{(3)} = \frac{5}{18} \frac{K_1^{(3)} K_3^{(3)}}{K_2^{(3)}}$

Table III. RG rules for the flow that starts in the green region ( $\tilde{S} = 2$ ) of the  $K^{(2)} \times K^{(3)}$  plane [see Fig. 6(c)].

system flow towards the pairwise random singlet case. This is illustrated in Fig. 7 where the length scale  $L$  (defined as the mean distance between effective spin clusters) is plotted along the RG flow parameterized by the cutoff energy scale  $\Omega$ . From this plot, the tunneling exponent  $\psi$  can be extracted by fitting the activated dynamical scaling law  $\ln \Omega \sim -L^\psi$ .

As discussed in Sec. VB, this triplewise random singlet phase is characteristic of integer spin- $S$  chains. In the case of  $S = 1$ , it was showed that the ground state exhibits an emergent SU(3) symmetry.<sup>11</sup> This is not the case, however, for the spin-2 chain. This can be explicitly verified by diagonalizing a system of 3 spins with  $K_i^{(3)} < 0$  and then computing the correlation function of the 24 SU(5) generators  $\Lambda_i^{(a)}$ ,  $i = 1, 2, 3$  and  $a = 1, \dots, 24$ , in the correspond singlet state. Choosing the normalization such that  $\text{Tr}(\Lambda^{(a)}\Lambda^{(b)}) = 2\delta^{a,b}$ , we find that

$$\left| \langle \Lambda_1^{(a)} \Lambda_2^{(a)} \rangle \right| = \frac{1}{35} \times \begin{cases} 7, & a = 1, 2, 3, \\ 3, & a = 4, \dots, 8, \\ 8, & a = 10, \dots, 15, \\ 4, & a = 16, \dots, 24. \end{cases} \quad (49)$$

The number of equal values follows exactly the degeneracies of the SU(2) multiplets. This implies that there is *no symmetry enhancement*: there is no symmetry higher than the obvious SU(2). This should be contrasted with the situation in the AF hyper-octant. In that region, the expectation value of all the SU(5) generators in the pairwise singlets is the same as at the SU(5) point

$$\left| \langle \Lambda_1^{(a)} \Lambda_2^{(a)} \rangle \right| = \frac{2}{5}, \quad a = 1, \dots, 24. \quad (50)$$

This should also be contrasted with the spin-1 case. An analogous computation [for the SU(3) group] of Eq. (49) shows that all expectation values are the same.<sup>11</sup> For the random spin-2 chain, by contrast, in the triplewise RSP where the singlets are mostly formed by spin trios, the symmetry remains SU(2) as in the bare Hamiltonian.

We now move to the analysis of the phases when ISTs of two different ranks are present in the initial Hamiltonian. In analogy with the spin-3/2 case (see Sec-

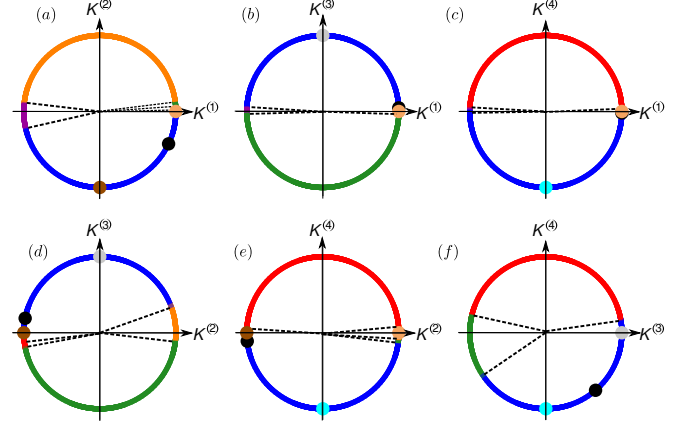


Figure 8. (Color online) Diagrams representing the 2-spin ground multiplet for two spins 2 and the AF RG fixed points of the disordered spin-2 chain in the various two-dimensional planes in  $\mathbf{K}$  space. The total angular momentum of the ground multiplets vary from  $\tilde{S} = 0$  to  $\tilde{S} = 4$  and it is identified by the color scheme of Table II. The small circles represent the AF angular fixed points. The stable AF ones lie on the semi-axes with  $K^{(1)} > 0, K^{(2)} < 0, K^{(3)} > 0$ , and  $K^{(3)} < 0$ . The unstable fixed points can also be found analytically (see the Appendix C).

tion VID), besides the stable fixed points on the semi-axes, some unstable planar fixed points exist in the AF hyper-octant, as discussed in Section VA. Both types of fixed points are shown in Fig. 9 and their precise locations are given in Table IV of Appendix C. The RG flow can be analyzed similarly to the spin  $\frac{3}{2}$  chain, with the additional presence of the  $\psi = \frac{1}{3}$  triplewise RSP. We outline some of the general results. Starting in the blue region leads to a  $\psi = \frac{1}{2}$  pairwise RSP, whereas starting in the green region leads to the  $\psi = \frac{1}{3}$  triplewise RSP. The purple region is purely FM, as indicated by the two-spin problem having  $\tilde{S} = 4$  as the local ground state. The red region, where  $\tilde{S} = 1$ , has to be analyzed in a case-by-case manner, leading, for instance, to a LSP, if  $K_i^{(1)}$  couplings are non-zero, as in the  $K^{(1)} \times K^{(3)}$  plane [see Fig. 8(b)], or to the breakdown of our RG scheme, as in the case of the  $K^{(3)} \times K^{(4)}$  plane [Fig. 8(f)]. In the latter, the RG fails because  $2\tilde{S} < 3$  and, therefore, both couplings are renormalized to zero at all RG steps. The orange region behaves similarly, leading also to vanishing coupling

constants [as in Fig. 8(d)] or to a LSP [as in Fig. 8(a)].

Finally, we focus on the 3-dimensional region spanned by the  $K^{(1)}$ ,  $K^{(2)}$  and  $K^{(3)}$  axes with  $K^{(4)} = 0$ , which is a 3-dimensional hyper-plane in  $\mathbb{R}^4$ . Other hyper-planes with  $K_i^{(4)} \neq 0$  yield qualitatively similar phase diagrams. We also remind the reader that, according to the analysis of Sec. V A, small  $K_i^{(4)}$  perturbations are irrelevant. Our results for the full RG flow, in analogy to the previous spin- $\frac{3}{2}$  case, are shown on a unit 2-sphere in the  $K^{(1)} \times K^{(2)} \times K^{(3)}$  space in Fig. 9. The fully stable AF fixed points on the semi-axes are shown as beige, brown and white circles. They define the AF hyper-octant (actually, the  $K^{(4)} = 0$  section of the hyper-octant). The semi-stable fixed points on the 2-planes [see panels (a), (b) and (d) of Fig. 9] are shown as black circles. The topology of the flow between these fixed points requires the existence of a third fixed point in the AF octant. It is shown as a pink circle, that is fully unstable on the surface of the unit 2-sphere. Note however that, unlike in the previous spin- $\frac{3}{2}$  case, this is not the totally unstable FP with enlarged SU(5) symmetry. The latter has  $K_i^{(4)} \neq 0$ , the precise location of which [see Appendix D for details about the SU( $N$ )-symmetric points] is given by

$$H_{5-5}^{\text{SU}(5)} = \sum_i K_i \left( \hat{O}_1 - \frac{4}{21} \hat{O}_2 + \frac{1}{21} \hat{O}_3 - \frac{4}{189} \hat{O}_4 \right) \quad (51)$$

The basins of attraction of the stable AF fixed points are found by a numerical analysis of the RG flow, following the same protocol as in the spin- $\frac{3}{2}$  chain. The results are summarized by the color-coded thick dots in the blue region of Fig. 9, where the colors used are the same as in the spin  $\frac{3}{2}$  chain in Fig. 4. Furthermore, the green dots map out the basin of attraction of the  $\psi = \frac{1}{3}$  fixed point along the  $K^{(3)}$  axis, which correspond to the triplewise RSP already discussed.

To conclude, we see that the phase diagram of the spin-2 chain differs *qualitatively* from the spin- $\frac{3}{2}$  case only due to the presence of the triplewise RSP with  $\psi = \frac{1}{3}$ . We expect the same trend to hold for disordered chains with higher spin values, with triplewise RSP appearing only in the cases of integer spins.

## VIII. SUMMARY OF RESULTS

In this Section, we summarize our main findings, focusing mostly on the different phases we have found as well as the conditions for their realization in the initial model but leaving out some of the technical details.

Our focus is on the SU(2)-symmetric, strongly disordered spin- $S$  chains. We have obtained general results for all values of  $S$  and have illustrated in full detail the cases of  $S = \frac{3}{2}$  and 2. Generic SU(2) symmetry (with only nearest-neighbor interactions, as we assume here) is usually identified by terms which only involve powers

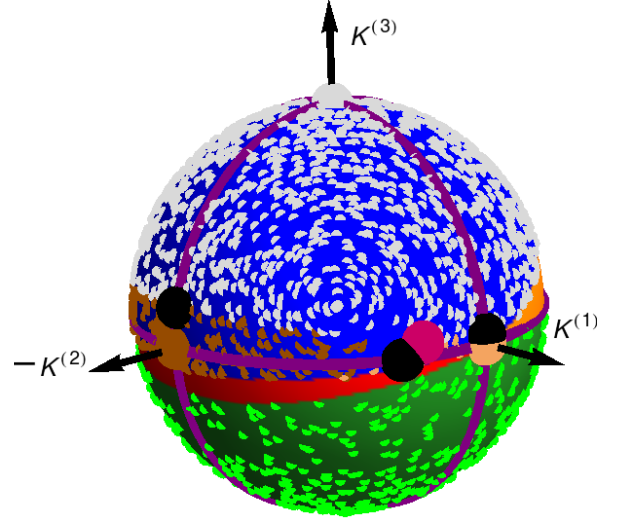


Figure 9. (Color online) Schematic phase/flow diagram of the disordered spin-2 chain on the unit 2-sphere of the hyper-space with  $K^{(4)} = 0$  and axes  $K^{(1)} \times K^{(2)} \times K^{(3)}$ . The regions on the sphere are colored according to the spin  $\tilde{S}$  of the ground multiplet of the 2-spin Hamiltonian, see Table II for the color scheme (the region with  $\tilde{S} = 4$  is not visible from this viewing angle). The thick dots on the sphere's surface represent initial conditions of the numerical RG flow, keeping always  $K_i^{(4)} = 0$ . A generic flow starting at a point in the blue region ends up at one of the stable fixed points on the semi-axes  $K^{(1)} > 0$ ,  $K^{(2)} < 0$ , and  $K^{(3)} > 0$  (dots have the same color as their final stable fixed points, which are represented by large circles on the semi-axes). Also in the blue region, semi-stable planar fixed points belonging to 2-planes (where only two  $K^{(J)}$  are non-zero) are represented in black. A single planar fixed point (belonging to the hyper-plane  $K^{(4)} = 0$ ) that is fully unstable on this 2-sphere is shown in pink. RG flows starting in the green region end up on a fixed point on the  $K^{(3)}$  axis with random signs, corresponding to the triplewise RSP with exponent  $\psi = \frac{1}{3}$ . The red and orange regions (not marked by any dot for clarity) are attracted to LSP fixed points.

of the scalar product of spin operators on adjacent sites; the largest power being  $J_{\text{max}} = 2S$ . There are  $J_{\text{max}}$  coupling constants per bond  $\alpha_i^{(J)}$  (with  $J = 1, 2, \dots, J_{\text{max}}$ ) between sites  $i$  and  $i + 1$ . This form of the Hamiltonian, however, is not the most suitable for an SDRG treatment. Instead, the flow becomes simpler if we rewrite the Hamiltonian in terms of scalars built by contractions of irreducible spherical tensors of spin operators of a given rank. We called them  $\hat{O}_J(\mathbf{S}_i, \mathbf{S}_{i+1})$ , where  $J$  is the rank of the tensors being contracted and again  $J = 1, 2, \dots, J_{\text{max}}$ . Each contraction has a coefficient  $K_i^{(J)}$ . The sets  $\alpha_i^{(J)}$  and  $K_i^{(J)}$  are linearly related, as shown for example in Eqs. (A9)-(A12) and (A13)-(A16).

If we think of the coupling constants as a vector  $\mathbf{K}_i = (K_i^{(1)}, \dots, K_i^{(J_{\text{max}})})$ , the SDRG transformations are then a set of rules that change the directions and magnitudes of these vectors, as well as the spin magnitude on each

site. In general, these three quantities are coupled in the earlier stages of the SDRG flow. Our results show, however, that the vector directions decouple from their magnitudes in the final stages of the flow (near the stable fixed points). This is the main reason why it is more convenient to rewrite the Hamiltonian in terms of the irreducible spherical tensors, namely, under the SDRG transformations, tensors of a given rank do not generate tensors of a different rank. This is a direct consequence of the  $SU(2)$  symmetry. We now summarize the SDRG flow.

Stable fixed points define stable extended phases. An important set of stable fixed points are the semi-axes  $(-1)^J K^{(J)} < 0$  (see Section V A and Fig. 3). The hyper-octant delimited by  $(-1)^J K^{(J)} < 0$  spans most (but not all) of its basin of attraction (see the blue regions of Figs. 4 and 9). If the system is such that all the vector directions are inside this basin of attraction and the spin sizes are uniform (equal to  $S$ ), then the RG flow is such that the spin sizes remain fixed and the vector directions flow towards one of the semi-axes  $(-1)^J K^{(J)} < 0$ . The main feature of these  $2S$  fixed points is that they define the *same* conventional pairwise random singlet state, which is a generalization of random singlet state of the spin-1/2 Heisenberg chain [see Fig. 2(a)]. The distribution of vector magnitudes tends towards a universal form with an asymptotically infinite relative width: a so-called infinite-randomness fixed point [see Eq. (27) with  $\psi = 1/2$ ]. The excitations correspond to the breaking of the singlet pairs in a hierarchy such that the relation between the energy  $E$  of a bond and its size  $\xi$  is given by  $E \sim \exp(-\xi^\psi)$ . Other physical properties follow from this structure. The magnetic susceptibility and specific heat behave as  $\chi^{-1} \sim T |\ln T|^{1/\psi}$  and  $C \sim |\ln T|^{1+1/\psi}$ , respectively. The average spin-spin correlation function decays as a power-law  $\langle \mathbf{S}_i \cdot \mathbf{S}_{i+r} \rangle \sim r^{-4\psi}$ . An important aspect of this set of fixed points is the emergence of an  $SU(2S+1)$  symmetry: correlation functions and susceptibilities of combinations of spin operators (dipolar, quadrupolar and other higher-multipole moments), which transform as generators of the  $SU(2S+1)$  group, are all equal in the limit of strong disorder. Finally, there must be unstable fixed points inside this basin of attraction. In particular, there is a completely unstable fixed point in a particular direction in  $\mathbf{K}_i$ -space lying within the hyper-octant with *exact*  $SU(2S+1)$  symmetry (see Fig. 5). At all fixed points within this basin of attraction, the ground state and the low-temperature thermodynamics are the same.

The second set of fixed points we have found happens for integer spins up to  $S = 9$ . As in the previous case, the spin size  $S$  remains constant along the RG flow. The vectors  $\mathbf{K}_i$ 's, however, do not point towards a single direction. Instead, they point towards the positive and negative directions of the axis  $J = I_S$ , with equal probability (where  $I_1 = 2$ , and  $I_S = 3$  for  $2 \leq S \leq 9$ , see Section V B). The corresponding phase is also a random-singlet phase. The singlets in this phase are formed by a

number of spins which is a multiplet of 3, with trios being the most abundant [see Fig. 2(b)]. As in the previous set of fixed points, it is also of the infinite-randomness type, sharing the same features (correlation functions and thermodynamics) but with an exponent  $\psi = 1/3$ . Its basin of attraction is illustrated by the green region in Fig. 9. Finally, there is no emergent symmetry at this fixed point larger than the original  $SU(2)$ , with the exception of the spin-1 case, for which there is an emergent  $SU(3)$  symmetry.<sup>11</sup>

A third important fixed point is found on the  $K_i^{(1)}$ -axis (the Heisenberg axis). As in the previous case, the vectors point (with approximately equal probability) towards both the positive (antiferromagnetic) and the negative (ferromagnetic)  $K^{(1)}$ -direction (see Section V C). Unlike the previous fixed points, the spin magnitude is not constant throughout the chain and the distribution of the vector magnitudes is of *finite*-randomness type [see Eq. (34)]. This implies a conventional scaling of energy and length scales  $\omega \sim \xi^{-z}$ , where  $z$  is the dynamical critical exponent. The coarse-grained degrees of freedom are spins of all sizes and the corresponding phase is named a Large Spin Phase.<sup>21</sup> The magnetic susceptibility is universal and Curie like  $\chi \sim T^{-1}$  while the specific heat behaves as  $C \sim T^z$ . For weakly disordered systems,  $z$  is universal and  $\approx 2.2$ . For strongly disordered systems,  $z$  is non-universal and depends on the disorder strength of the initial vector magnitude distribution.

The basins of attraction of these three classes of fixed points above exhaust the parameter space except for the regions with FM long-range order and other regions of measure zero. Therefore, in the strong disorder limit, the phase diagram displays four phases whenever  $S \leq 9$  and integer: the pairwise and triplewise random singlet phases, the FM phase, and the Large Spin phase (see Fig. 9 for the  $S = 2$  case, and Fig. 1 of Ref. 11 for the  $S = 1$  case). For the remaining cases (half-integer spins or  $S > 9$ ), the phase diagram shows the same phases with the exception of the triplewise random singlet phase (see Fig. 4).

## IX. OUTLOOK

In this section, we comment on some open questions and give some perspective for future directions of research.

Let us start with a technical open issue. Our method is able to produce an RG flow in the whole parameter space of the Hamiltonian (9) except for a zero-measure set as discussed in Sec. VI C. This peculiar set of parameters is a subset of the  $K_i^{(1)} = 0$  hyper-plane (see details in Sec. VI C) in which first-order perturbation theory fails to produce non-vanishing corrections in the SDRG decimation procedure. Although the RG flow is well-behaved outside this hyper-plane, it would be desirable to know the real fate of the flow in this hyper-plane. At the moment, it is unclear whether including higher-order per-

turbative terms in the decimation procedure will suffice to produce a consistent RG flow or whether there is new physics in this set of parameters.

Our approach is based on a strong-disorder RG method which becomes asymptotically exact near infinite-randomness fixed points. We have found two sets of such fixed points (corresponding to the pairwise and triplewise RSP) and a set of finite-disorder fixed points (corresponding to the Large Spin phase). Naturally, our approach cannot give exact results in the Large Spin phase. Unfortunately, there are no studies on the precision of the SDRG method at finite-disorder fixed points except for one study in which the accuracy of the SDRG method is shown to be within 1% (for the values of some critical exponents) when the dynamical critical exponent is greater than modest values  $\approx 1.5$ .<sup>36</sup> We have not performed an analysis of the dynamical critical exponent dependence on the initial conditions and leave this task for the future. It is known to be different from the one reported in Ref. 21 when other terms beyond the usual nearest-neighbor Heisenberg interactions are present.<sup>37</sup> In addition, as pointed out in Ref. 11, there are regions in which three phases meet. A complete analysis of the corresponding unstable critical points is also left as an open question. Finally, we remind that our method can neither capture the phases of the clean system nor predict if they are stable against weak disorder. For the latter one, other methods are necessary (see discussion in Ref. 11 for the  $S = 1$  case). Thus, there is the possibility of a much richer phase diagram in the intermediate disorder regime.

One particular outcome of our results concerns the so-called permutation-symmetric multicritical points.<sup>8</sup> In spin- $S$  random chains, it was shown that whenever  $N_1 = 2S + 1$  different dimerized phases meet at a single multicritical point, this point is of infinite-randomness type with tunneling exponent  $\psi = 1/N_1$ . At that point, it was left as an open question what is the (fine-tuned) condition necessary for these phases to meet at a single point. As we have shown here, there are no phases with arbitrarily small tunneling exponent. Such feature only happens at special unstable fixed points which possess explicit  $SU(N)$  symmetry (with  $N = N_1$ ) and which we have shown how to precisely define. Therefore, we have now discovered the exact location of the permutation-symmetric multicritical points in  $SU(2)$ -symmetric spin- $S$  random chains: they occur at the  $SU(2S + 1)$ -symmetric point.

As mentioned in the Introduction, the main motivation

for this work is the search for phases displaying emergent enlarged symmetries and the understanding of the corresponding physical mechanism. Indeed, we have found an emergent  $SU(2S + 1)$  symmetry in the entire pairwise RSP. In addition, this phase is pairwise, and thus,  $\psi = 1/2$  (a “mesonic” phase). As shown in Ref. 11, the triplewise RSP of the spin-1 chain also possesses an emergent  $SU(3)$  symmetry, with  $\psi = 1/3$  (a “baryonic” phase). Unfortunately, we have not found a generalization of the baryonic RSP for higher spins. This would be interesting because it would imply in the existence of entire phases with  $\psi = (2S + 1)^{-1}$ . We have found instead some triplewise RSPs for integer spins  $S$  with  $2 \leq S \leq 9$ , which, however, do not possess any enhanced symmetry. In some sense, this supports the conventional wisdom that emergent enhanced symmetries are indeed more the exception than the rule. Additionally, a line with  $SO(5)$  symmetry was found in the spin-3/2 random chains which contains the corresponding  $SU(4)$  baryonic and mesonic points. Since it is confined to a lower dimensional manifold of the full phase space, it suggests that an emergent  $SU(2S + 1)$  baryonic RSP may be realized in a different symmetry group. Exploring spin chain Hamiltonians with  $SO(N)$  symmetry is the next step of our research. This is not of just academic curiosity since experimental realizations of these groups have been proposed in cold-atomic systems.<sup>13,15</sup>

Finally, we point out that our method has exciting applications to the Hamiltonian in Eq. (1) generalized to any dimension, geometry (as in ladders) or with long-range interactions. For instance, in higher dimensions there are quantum phase transitions between the Néel AFM state to other phases (such as a valence bond crystal phase) upon increasing the value of the terms besides the bilinear one. Our method can thus be directly used to study the disorder effects on such quantum phase transitions.

## X. ACKNOWLEDGMENTS

We gratefully acknowledge P. L. S. Lopes for useful discussions. This work has been supported by FAPESP through grants 2009/17531-3 (VLQ), 07/57630-5 (EM) and 2015/23849-7 (JAH), and by CNPq through grants 307548/2015-5 (JHA), 304311/2010-3 (EM) and 590093/2011-8 (JHA and EM).

## Appendix A: Dictionary of conversion of different notations

In this Appendix, we list several conversions between different forms of the relevant operators and Hamiltonians used in the paper. The calculations are tedious but straightforward. Alternatively, the use of a software like MATHEMATICA expedites the procedure.



We first explicitly show the decomposition of  $(\mathbf{S}_1 \cdot \mathbf{S}_2)^J$ , for  $J = 1, \dots, 4$ , in terms of the  $\hat{O}_J$  operators

$$(\mathbf{S}_1 \cdot \mathbf{S}_2) = \frac{4\pi}{3} \hat{O}_1, \quad (\text{A1})$$

$$(\mathbf{S}_1 \cdot \mathbf{S}_2)^2 = -\frac{2\pi}{3} \hat{O}_1 + \frac{8\pi}{15} \hat{O}_2 + \frac{1}{3} \mathbf{S}_1^2 \mathbf{S}_2^2, \quad (\text{A2})$$

$$(\mathbf{S}_1 \cdot \mathbf{S}_2)^3 = \left( -\frac{8\pi}{30} (\mathbf{S}_1^2 + \mathbf{S}_2^2 - 3\mathbf{S}_1^2 \mathbf{S}_2^2) + \frac{8\pi}{15} \right) \hat{O}_1 - \frac{16\pi}{15} \hat{O}_2 + \frac{8\pi}{35} \hat{O}_3 - \frac{1}{6} \mathbf{S}_1^2 \mathbf{S}_2^2, \quad (\text{A3})$$

$$\begin{aligned} (\mathbf{S}_1 \cdot \mathbf{S}_2)^4 = & \frac{2\pi}{3} (\mathbf{S}_1^2 + \mathbf{S}_2^2 - 2\mathbf{S}_1^2 \mathbf{S}_2^2 - 1) \hat{O}_1 + \frac{8\pi}{105} (31 - 5\mathbf{S}_1^2 - 5\mathbf{S}_2^2 + 6\mathbf{S}_1^2 \mathbf{S}_2^2) \hat{O}_2 - \frac{8\pi}{7} \hat{O}_3 + \frac{32\pi}{315} \hat{O}_4 \\ & + \frac{2}{15} \mathbf{S}_1^2 \mathbf{S}_2^2 - \frac{1}{15} (\mathbf{S}_1^4 \mathbf{S}_2^2 + \mathbf{S}_1^2 \mathbf{S}_2^4) + \frac{1}{5} \mathbf{S}_1^4 \mathbf{S}_2^4. \end{aligned} \quad (\text{A4})$$

Conversely,

$$\hat{O}_1 = \frac{3}{4\pi} (\mathbf{S}_1 \cdot \mathbf{S}_2), \quad (\text{A5})$$

$$\hat{O}_2 = \frac{15}{16\pi} (\mathbf{S}_1 \cdot \mathbf{S}_2) + \frac{15}{8\pi} (\mathbf{S}_1 \cdot \mathbf{S}_2)^2 - \frac{5}{8\pi} \mathbf{S}_1^2 \mathbf{S}_2^2, \quad (\text{A6})$$

$$\hat{O}_3 = \frac{7}{8\pi} (\mathbf{S}_1^2 + \mathbf{S}_2^2 - 3\mathbf{S}_1^2 \mathbf{S}_2^2 + 3) (\mathbf{S}_1 \cdot \mathbf{S}_2) + \frac{35}{4\pi} (\mathbf{S}_1 \cdot \mathbf{S}_2)^2 + \frac{35}{8\pi} (\mathbf{S}_1 \cdot \mathbf{S}_2)^3 - \frac{35}{16\pi} \mathbf{S}_1^2 \mathbf{S}_2^2, \quad (\text{A7})$$

$$\begin{aligned} \hat{O}_4 = & -\frac{45}{32\pi} (17\mathbf{S}_1^2 \mathbf{S}_2^2 - 6(\mathbf{S}_1^2 + \mathbf{S}_2^2) - 9) (\mathbf{S}_1 \cdot \mathbf{S}_2) - \frac{45}{32\pi} (6\mathbf{S}_1^2 \mathbf{S}_2^2 - 5(\mathbf{S}_1^2 + \mathbf{S}_2^2) - 39) (\mathbf{S}_1 \cdot \mathbf{S}_2)^2 \\ & + \frac{1575}{32\pi} (\mathbf{S}_1 \cdot \mathbf{S}_2)^3 + \frac{315}{32\pi} (\mathbf{S}_1 \cdot \mathbf{S}_2)^4 - \frac{729}{64\pi} \mathbf{S}_1^2 \mathbf{S}_2^2 - \frac{27}{16\pi} (\mathbf{S}_1^2 \mathbf{S}_2^4 + \mathbf{S}_1^4 \mathbf{S}_2^2) + \frac{27}{32\pi} \mathbf{S}_1^4 \mathbf{S}_2^4. \end{aligned} \quad (\text{A8})$$

The coupling constants can be mapped according to

$$\alpha^{(1)} = \frac{1}{16\pi} \left( 12K^{(1)} + 15K^{(2)} + 14(3 + \mathbf{S}_1^2 + \mathbf{S}_2^2 - 3\mathbf{S}_1^2 \mathbf{S}_2^2) K^{(3)} \right) + \left( \frac{405}{32\pi} + \frac{135}{16\pi} (\mathbf{S}_1^2 + \mathbf{S}_2^2) - \frac{765}{32\pi} \mathbf{S}_1^2 \mathbf{S}_2^2 \right) K^{(4)} \quad (\text{A9})$$

$$\alpha^{(2)} = \frac{5}{8\pi} \left( 3K^{(2)} + 14K^{(3)} \right) + \left( \frac{1755}{32\pi} + \frac{225}{32\pi} (\mathbf{S}_1^2 + \mathbf{S}_2^2) - \frac{135}{16\pi} \mathbf{S}_1^2 \mathbf{S}_2^2 \right) K^{(4)}, \quad (\text{A10})$$

$$\alpha^{(3)} = \frac{35}{8\pi} K^{(3)} + \frac{1575}{32\pi} K^{(4)}, \quad (\text{A11})$$

$$\alpha^{(4)} = \frac{315}{32\pi} K^{(4)}, \quad (\text{A12})$$

and

$$K^{(1)} = \frac{4\pi}{3} \alpha^{(1)} - \frac{2\pi}{3} \alpha^{(2)} - \frac{8\pi}{30} (\mathbf{S}_1^2 + \mathbf{S}_2^2 - 3\mathbf{S}_1^2 \mathbf{S}_2^2 - 2) \alpha^{(3)} + \frac{2\pi}{3} (\mathbf{S}_1^2 + \mathbf{S}_2^2 - 2\mathbf{S}_1^2 \mathbf{S}_2^2 - 1) \alpha^{(4)}, \quad (\text{A13})$$

$$K^{(2)} = \frac{8\pi}{15} \alpha^{(2)} - \frac{16\pi}{15} \alpha^{(3)} + \frac{8\pi}{105} (31 - 5\mathbf{S}_1^2 - 5\mathbf{S}_2^2 + 6\mathbf{S}_1^2 \mathbf{S}_2^2) \alpha^{(4)}, \quad (\text{A14})$$

$$K^{(3)} = \frac{8\pi}{35} \alpha^{(3)} - \frac{8\pi}{7} \alpha^{(4)}, \quad (\text{A15})$$

$$K^{(4)} = \frac{32\pi}{315} \alpha^{(4)}. \quad (\text{A16})$$

Also relevant is the decomposition of projection operators into spin objects. Unlike the previous equations, which can be found for any values of  $\mathbf{S}_2$  and  $\mathbf{S}_3$ , this has to be done in a case-by-case manner. For two coupled spin  $\frac{3}{2}$ , we

find the following correspondence

$$\epsilon^{(0)} = \alpha^{(0)} - \frac{15}{4}\alpha^{(1)} + \frac{225}{16}\alpha^{(2)} - \frac{3375}{64}\alpha^{(3)}, \quad (\text{A17})$$

$$\epsilon^{(1)} = \alpha^{(0)} - \frac{11}{4}\alpha^{(1)} + \frac{121}{16}\alpha^{(2)} - \frac{1331}{64}\alpha^{(3)}, \quad (\text{A18})$$

$$\epsilon^{(2)} = \alpha^{(0)} - \frac{3}{4}\alpha^{(1)} + \frac{9}{16}\alpha^{(2)} - \frac{25}{64}\alpha^{(3)}, \quad (\text{A19})$$

$$\epsilon^{(3)} = \alpha^{(0)} + \frac{9}{4}\alpha^{(1)} + \frac{81}{16}\alpha^{(2)} + \frac{729}{64}\alpha^{(3)}, \quad (\text{A20})$$

and, conversely,

$$K^{(0)} = \frac{\pi}{4}\epsilon^{(0)} - \frac{3\pi}{4}\epsilon^{(1)} + \frac{5\pi}{4}\epsilon^{(2)} + \frac{7\pi}{4}\epsilon^{(3)}, \quad (\text{A21})$$

$$K^{(1)} = -\frac{\pi}{15}\epsilon^{(0)} - \frac{11\pi}{75}\epsilon^{(1)} - \frac{\pi}{15}\epsilon^{(2)} + \frac{7\pi}{25}\epsilon^{(3)}, \quad (\text{A22})$$

$$K^{(2)} = \frac{\pi}{45}\epsilon^{(0)} + \frac{\pi}{75}\epsilon^{(1)} - \frac{\pi}{15}\epsilon^{(2)} + \frac{7\pi}{225}\epsilon^{(3)}, \quad (\text{A23})$$

$$K^{(3)} = -\frac{4\pi}{315}\epsilon^{(0)} + \frac{4\pi}{175}\epsilon^{(1)} - \frac{4\pi}{315}\epsilon^{(2)} + \frac{4\pi}{1575}\epsilon^{(3)}. \quad (\text{A24})$$

## Appendix B: Derivation of the RG step

In this Appendix, we give details about the perturbative calculations that allow one to make one RG decimation step. We divide this Appendix into three subsections. In the first and second subsections, we derive how the first- and second-order perturbation theories are applied to this problem, while the details about the calculation of coefficients that appear in the first two subsections are left for the final subsection.

Throughout this derivation, we will need to compute matrix elements of ISTs in a two-site problem. Let us then already set the notation we are going to follow. The notation is the same as in Edmonds' book<sup>23</sup> (see, for instance, page 74). Assume that the largest energy gap is due to a bond connecting sites 2 and 3 and let us call the spins of this 2-site problem  $\mathbf{S}_2$  and  $\mathbf{S}_3$ . The Wigner-Eckart theorem, that gives the matrix elements of ISTs of rank  $J$  and component  $M$ ,  $Y_{JM}(\mathbf{S}_i)$  ( $i = 2, 3$ ) in the total angular momentum basis, is given by

$$\langle S_2 S_3, J' M' | Y_{JM}(\mathbf{S}_i) | S_2 S_3, J'' M'' \rangle = (-1)^{J-J'+J''} \frac{\langle J J''; M M'' | J J''; J' M' \rangle}{\sqrt{2J'+1}} \langle S_2 S_3, J' || Y_J(\mathbf{S}_i) || S_2 S_3, J'' \rangle, \quad (\text{B1})$$

where  $\langle J' || Y_J(\mathbf{S}) || J \rangle$  is the reduced matrix element, independent of the IST component  $M$  component and the angular momentum projections  $M'$  and  $M''$ . To simplify the notation, in this Appendix we write  $\langle S_2 S_3 J' || Y_J(\mathbf{S}_i) || S_2 S_3 J'' \rangle \equiv \langle J' || Y_J(\mathbf{S}_i) || J'' \rangle$ .

### 1. First-order perturbation theory

The algebraic challenge is to simplify the projection defined in the main text in Eq. (15), i. e., to find effective couplings between  $S_1$  and the new spin  $\tilde{S}$ , introduced to replace  $S_2$  and  $S_3$ , at low energies. For concreteness, we focus on operators of site 2,  $Y_{J-M}(\mathbf{S}_2)$ . By using the projection operator onto a multiplet of total angular momentum  $\tilde{S}$ , as defined in Eq. (10),

$$P_{\tilde{S}} = \sum_{M'=-\tilde{S}}^{\tilde{S}} |\tilde{S} M'\rangle \langle \tilde{S} M'|, \quad (\text{B2})$$

we find the projection to be

$$\begin{aligned}
P_{\tilde{S}} Y_{J-M}(\mathbf{S}_2) P_{\tilde{S}} &= \left( \sum_{M'} |\tilde{S}M'\rangle \langle \tilde{S}M'| \right) Y_{J-M}(\mathbf{S}_2) \left( \sum_{M''} |\tilde{S}M''\rangle \langle \tilde{S}M''| \right), \\
&= \sum_{M', M''} |\tilde{S}M'\rangle \langle \tilde{S}M''| \langle \tilde{S}M' | Y_{J-M}(\mathbf{S}_2) | \tilde{S}M'' \rangle,
\end{aligned} \tag{B3}$$

We now apply the Wigner-Eckart theorem, Eq. (B1), in order to calculate the matrix element  $\langle \tilde{S}M' | Y_{J-M}(\mathbf{S}_2) | \tilde{S}M'' \rangle$ . This matrix element is proportional to  $\langle \tilde{S} || Y_J(\mathbf{S}_2) || \tilde{S} \rangle$  and to the Clebsch-Gordan coefficient  $\langle J\tilde{S}; -MM'' | J\tilde{S}; \tilde{S}M' \rangle$ . In order to rewrite the projection as a new IST acting on the ground state manifold, we use the Wigner-Eckart theorem again to calculate  $\langle \tilde{S}M' | Y_{J-M}(\tilde{\mathbf{S}}) | \tilde{S}M'' \rangle$ , where  $\mathbf{S}_2$  has been replaced by  $\tilde{\mathbf{S}}$ . The latter is proportional to  $\langle \tilde{S} || Y_J(\tilde{\mathbf{S}}) || \tilde{S} \rangle$  and to the same Clebsch-Gordan coefficient, which implies

$$\frac{\langle \tilde{S}M' | Y_{J-M}(\mathbf{S}_2) | \tilde{S}M'' \rangle}{\langle \tilde{S}M' | Y_{J-M}(\tilde{\mathbf{S}}) | \tilde{S}M'' \rangle} = \frac{\langle \tilde{S} || Y_J(\mathbf{S}_2) || \tilde{S} \rangle}{\langle \tilde{S} || Y_J(\tilde{\mathbf{S}}) || \tilde{S} \rangle}. \tag{B4}$$

Therefore, we get

$$P_{\tilde{S}} Y_{J-M}(\mathbf{S}_2) P_{\tilde{S}} = \frac{\langle \tilde{S} || Y_J(\mathbf{S}_2) || \tilde{S} \rangle}{\langle \tilde{S} || Y_J(\tilde{\mathbf{S}}) || \tilde{S} \rangle} \sum_{M'} \sum_{M''} |\tilde{S}M'\rangle \langle \tilde{S}M' | Y_{J-M}(\tilde{\mathbf{S}}) | \tilde{S}M'' \rangle \langle \tilde{S}M''|, \tag{B5}$$

$$= \frac{\langle \tilde{S} || Y_J(\mathbf{S}_2) || \tilde{S} \rangle}{\langle \tilde{S} || Y_J(\tilde{\mathbf{S}}) || \tilde{S} \rangle} P_{\tilde{S}} Y_{J-M}(\tilde{\mathbf{S}}) P_{\tilde{S}}. \tag{B6}$$

$$= f^{(J)}(S_2, S_3, \tilde{S}) P_{\tilde{S}} Y_{J-M}(\tilde{\mathbf{S}}) P_{\tilde{S}}. \tag{B7}$$

This is a fundamental part of the process, which guarantees that the renormalized Hamiltonian has the same functional form as the undecimated one. We leave the calculation of the ratio of reduced matrix elements  $f^{(J)}(S_2, S_3, \tilde{S})$  to the third part of this Appendix. The new coupling is, therefore,

$$\tilde{K}_1^{(J)} = f^{(J)}(S_2, S_3, \tilde{S}) K_1^{(J)}. \tag{B8}$$

For the effective coupling between  $\tilde{S}$  and  $S_3$ , the calculation can be done following the same steps with the replacement  $S_2 \rightleftharpoons S_3$ . Therefore,

$$\tilde{K}_3^{(J)} = f^{(J)}(S_3, S_2, \tilde{S}) K_3^{(J)}. \tag{B9}$$

## 2. Second-order perturbation theory

In the main text, we gave some of the steps for the second-order perturbation theory calculation. Particularly, we showed that selection rules restrict the values of the angular momentum of virtual states in such a way that we are left with the task of computing  $\langle 00 | Y_{J-M}(\mathbf{S}_2) | JM \rangle \langle JM | Y_{JM}(\mathbf{S}_3) | 00 \rangle$ . In this section, we want to justify the simplification we made from Eq. (24) to Eq. (25), that is, the  $M$ -independence of  $g(J, S)$ . From the Wigner-Eckart theorem, Eq. (B1), the  $M$ -dependence of the product  $\langle 00 | Y_{J-M}(\mathbf{S}_2) | JM \rangle \langle JM | Y_{JM}(\mathbf{S}_3) | 00 \rangle$  is given by the product of the Clebsch-Gordan coefficients  $\langle JJ; -MM | JJ; 00 \rangle$  and  $\langle J0; M0 | J0; JM \rangle$ , since both the pre-factor and the reduced matrix elements are  $M$ -independent. These Clebsch-Gordan coefficients can be explicitly calculated, and are equal to

$$\langle JJ; -MM | JJ; 00 \rangle = \frac{(-1)^{J+M}}{\sqrt{1+2J}}, \tag{B10}$$

$$\langle J0; M0 | J0; JM \rangle = 1. \tag{B11}$$

The  $M$ -dependence is, then,  $(-1)^M$ , and

$$\langle 00 | Y_{J-M}(\mathbf{S}_2) | JM \rangle \langle JM | Y_{JM}(\mathbf{S}_3) | 00 \rangle = (-1)^M g(J, S), \tag{B12}$$

as defined in the main text. The function  $g$  is going to be calculated in the next part of this Appendix.

### 3. Reduced matrix element calculations

#### a. Reduced matrix elements of ISTs

We now need to find analytic expressions for the reduced matrix elements. There is a great simplification in the cases we treat in this paper, in which the operators act only on the degrees of freedom of one of the sites, as shown in Ref. 23 (page 111),

$$\langle J' || Y_J(\mathbf{S}_2) || J'' \rangle = (-1)^{S_2+S_3+J''+J} \sqrt{(2J'+1)(2J''+1)} \left\{ \begin{matrix} S_2 & J' & S_3 \\ J'' & S_2 & J \end{matrix} \right\} \langle S_2 || Y_J(\mathbf{S}_2) || S_2 \rangle, \quad (\text{B13})$$

where  $\{...\}$  represents the Wigner's  $6-j$  symbol, and analogously for the reduced matrix elements of  $Y_J(\mathbf{S}_3)$ . The reduced matrix element above,  $\langle S_2 || Y_J(\mathbf{S}_2) || S_2 \rangle$ , can be easily calculated by going back to the Wigner-Eckart theorem, Eq. (B1), and choosing the state with highest possible value of  $M$ ,  $M = S$ , and  $J' = J'' = S_2$ ,

$$\langle S_2 || Y_J(\mathbf{S}_2) || S_2 \rangle = (-1)^J \sqrt{2S_2+1} \frac{\langle S_2 S_2 | Y_{J0} | S_2 S_2 \rangle}{\langle J S_2; 0 S_2 | J S_2; S_2 S_2 \rangle}. \quad (\text{B14})$$

#### b. First-order perturbation theory

The ratio of reduced matrix elements is what is left in the first-order perturbation theory calculation [Eq. (B16)]. The numerator  $\langle \tilde{S} || Y_J(\mathbf{S}_2) || \tilde{S} \rangle$  corresponds to the case when  $J'' = J' = \tilde{S}$  of Eq. (B13). The denominator is the reduced matrix element  $\langle \tilde{S} || Y_J(\tilde{\mathbf{S}}) || \tilde{S} \rangle$ , that can be easily calculated from the Wigner-Eckart theorem, Eq. (B1), by again choosing  $J'' = J' = \tilde{S}$

$$\langle \tilde{S} || Y_J(\tilde{\mathbf{S}}) || \tilde{S} \rangle = \frac{(-1)^J \sqrt{2\tilde{S}+1} \langle \tilde{S} \tilde{S} | Y_{J0}(\tilde{\mathbf{S}}) | \tilde{S} \tilde{S} \rangle}{\langle J \tilde{S}; 0 \tilde{S} | J \tilde{S}; \tilde{S} \tilde{S} \rangle}. \quad (\text{B15})$$

After some simplifications, we get

$$\frac{\langle \tilde{S} || Y_J(\mathbf{S}_2) || \tilde{S} \rangle}{\langle \tilde{S} || Y_J(\tilde{\mathbf{S}}) || \tilde{S} \rangle} = (-1)^{S_2+S_3+\tilde{S}+J} \frac{(2\tilde{S}+1)!}{(2S_2)!} \sqrt{\frac{(2S_2-J)!(2S_2+J+1)!}{(2\tilde{S}-J)!(2\tilde{S}+J+1)!}} \left\{ \begin{matrix} S_2 & \tilde{S} & S_3 \\ \tilde{S} & S_2 & J \end{matrix} \right\} \frac{\langle S_2 S_2 | Y_{J0}(\mathbf{S}_2) | S_2 S_2 \rangle}{\langle \tilde{S} \tilde{S} | Y_{J0}(\tilde{\mathbf{S}}) | \tilde{S} \tilde{S} \rangle} \quad (\text{B16})$$

where the last term of the right-hand side is

$$\frac{\langle S_2 S_2 | Y_{J0}(\mathbf{S}_2) | S_2 S_2 \rangle}{\langle \tilde{S} \tilde{S} | Y_{J0}(\tilde{\mathbf{S}}) | \tilde{S} \tilde{S} \rangle} = \frac{\prod_{S=\{0, \frac{1}{2}, \dots, \frac{J-1}{2}\}} (S_2 - S)}{\prod_{S=\{0, \frac{1}{2}, \dots, \frac{J-1}{2}\}} (\tilde{S} - S)}. \quad (\text{B17})$$

Putting it all together, we find

$$f^{(J)}(S_2, S_3, \tilde{S}) = \frac{\langle \tilde{S} || Y_J(\mathbf{S}_2) || \tilde{S} \rangle}{\langle \tilde{S} || Y_J(\tilde{\mathbf{S}}) || \tilde{S} \rangle} \quad (\text{B18})$$

$$= (-1)^{S_2+S_3+\tilde{S}+J} \frac{(2\tilde{S}+1)!}{(2S_2)!} \sqrt{\frac{(2S_2-J)!(2S_2+J+1)!}{(2\tilde{S}-J)!(2\tilde{S}+J+1)!}} \left\{ \begin{matrix} S_2 & \tilde{S} & S_3 \\ \tilde{S} & S_2 & J \end{matrix} \right\} \frac{\prod_{S < J-1} (S_2 - S)}{\prod_{S < J-1} (\tilde{S} - S)}. \quad (\text{B19})$$

Using the properties of the  $6-j$  symbol, we also find (page 94 of Ref. 23)

$$\left\{ \begin{matrix} S_2 & \tilde{S} & S_3 \\ \tilde{S} & S_2 & J \end{matrix} \right\} = \left\{ \begin{matrix} \tilde{S} & \tilde{S} & J \\ S_2 & S_2 & S_3 \end{matrix} \right\}. \quad (\text{B20})$$

A necessary condition for the above  $6-j$  symbol above to be *non-zero* is that the so-called triangular conditions are satisfied by  $(\tilde{S}, \tilde{S}, J)$  and  $(S_2, S_2, J)$ . A triad  $(l_1, l_2, l_3)$  is said to satisfy a triangular condition when it is possible to build a triangle with edges of sizes  $l_1$ ,  $l_2$  and  $l_3$ . The triad  $(\tilde{S}, \tilde{S}, J)$  satisfies the triangular condition if, and only if,



$J < 2\tilde{S}$ . In one case discussed in the main text,  $S_2 = S_3 = \frac{3}{2}$ ,  $\tilde{S} = 1$ , and  $J = 3$ , this condition is not satisfied. That is what we have called case (a) in Section III 1. The second triangular condition is equivalent to  $S_2 < 2\tilde{S}$ , and is always satisfied. On the other hand, in another case discussed in the main text,  $S_2 = S_3 = \frac{3}{2}$  again, but  $\tilde{S} = 2$  and  $J = 2$ . Even though the triangular conditions are satisfied, the  $\delta$ - $j$  symbol in Eq. (B20) vanishes. This is what we have called case (b) in Section III 1. Its occurrence cannot be predicted in general.

### c. Second-order perturbation theory

Now, we go back to the second-order perturbation theory calculation and find explicitly the  $g(J, S)$  function. The difference when compared to first order perturbation theory is that the matrix elements of Eq. (23) are calculated between a state of finite angular momentum and a singlet. The matrix elements are, using Eqs. (B1), (B13) and (B14)

$$\begin{aligned}\langle 00 | Y_{J-M}(\mathbf{S}_2) | JM \rangle &= (-1)^{J+2S} \frac{\langle JJ; -MM | JJ; 00 \rangle}{\langle JS; 0S | JS; SS \rangle} \sqrt{(2J+1)(2S+1)} \begin{Bmatrix} S & 0 & S \\ J & S & J \end{Bmatrix} \langle SS | Y_{J0} | SS \rangle, \\ \langle JM | Y_{JM}(\mathbf{S}_3) | 00 \rangle &= (-1)^{J+2S} \frac{\langle J0; M0 | J0; JM \rangle}{\langle JS; 0S | JS; SS \rangle} \sqrt{(2J+1)(2S+1)} \begin{Bmatrix} S & J & S \\ 0 & S & J \end{Bmatrix} \langle SS | Y_{J0} | SS \rangle.\end{aligned}$$

Multiplying the previous equations and simplifying the  $\delta$ - $j$  symbol, we get

$$g(J, S) = (-1)^J \left( \frac{1+2S}{1+2J} \right) \frac{(2S-J)!(2S+J+1)!}{(2S+1)!(2S+1)!} |\langle SS | Y_{J0} | SS \rangle|^2 \quad (\text{B21})$$

The matrix elements that are explicitly used in this manuscript are

$$\langle S, S | Y_{10} | S, S \rangle = \frac{1}{2} \sqrt{\frac{3}{\pi}} S, \quad (\text{B22})$$

$$\langle S, S | Y_{20} | S, S \rangle = \frac{1}{2} \sqrt{\frac{5}{\pi}} S \left( S - \frac{1}{2} \right), \quad (\text{B23})$$

$$\langle S, S | Y_{30} | S, S \rangle = \frac{1}{2} \sqrt{\frac{7}{\pi}} S \left( S - \frac{1}{2} \right) (S-1), \quad (\text{B24})$$

$$\langle S, S | Y_{40} | S, S \rangle = \frac{3}{2} \sqrt{\frac{1}{\pi}} S_2 \left( S_2 - \frac{1}{2} \right) (S_2-1) \left( S_2 - \frac{3}{2} \right). \quad (\text{B25})$$

Note that the matrix elements are zero if  $S < \frac{J}{2}$ , which immediately implies a product of  $S - S_i$ , with  $S_i < S$ . The only task for higher rank tensors is, then, to find the overall prefactors.

Explicitly, for the tensors studied in this paper,

$$g(1, S) = -\frac{(S+1)S}{4\pi}, \quad (\text{B26})$$

$$g(2, S) = \frac{(S+\frac{3}{2})(S+1)S(S-\frac{1}{2})}{4\pi}, \quad (\text{B27})$$

$$g(3, S) = -\frac{(S+2)(S+\frac{3}{2})(S+1)S(S-\frac{1}{2})(S-1)}{4\pi}, \quad (\text{B28})$$

$$g(4, S) = \frac{(S+\frac{5}{2})(S+2)(S+\frac{3}{2})(S+1)S(S-\frac{1}{2})(S-1)(S-\frac{3}{2})}{4\pi}. \quad (\text{B29})$$

The above equations suggest a general formula for  $g(J, S)$ , which, however, we were not able to prove

$$g(J, S) = \frac{(-1)^J}{4\pi} \frac{(2S+1+J)!}{2^{2J}(2S-J)!}, \quad (\text{B30})$$

$$= \frac{(-1)^J}{4\pi} \left( S + \frac{J+1}{2} \right) \left( S + \frac{J}{2} \right) \dots (S+1) S \left( S - \frac{1}{2} \right) \dots \left[ S - \frac{(J-1)}{2} \right]. \quad (\text{B31})$$

Plane	Planar Fixed Point
$K^{(1)} \times K^{(2)}$	$K^{(2)} = -\frac{4}{735} (39 + 4\sqrt{141}) K^{(1)}, K^{(1)} > 0$
$K^{(1)} \times K^{(3)}$	$K^{(3)} = \frac{1}{21} K^{(1)}, K^{(1)} > 0$
$K^{(1)} \times K^{(4)}$	$K^{(4)} = -\frac{2}{19845} (59 + \sqrt{18181}) K^{(1)}, K^{(1)} > 0$
$K^{(2)} \times K^{(3)}$	$K^{(3)} = \frac{1}{56} (1 - \sqrt{141}) K^{(2)}, K^{(2)} < 0$
$K^{(4)} \times K^{(2)}$	$K^{(4)} = \frac{1}{9} K^{(2)}, K^{(2)} < 0$
$K^{(4)} \times K^{(3)}$	$K^{(4)} = -\frac{1175 - \sqrt{2328145}}{1080} K^{(2)}, K^{(4)} < 0$

Table IV. Planar fixed points of the disordered spin-2 chain.

### Appendix C: RG decimation rules: Spin $\frac{3}{2}$ and Spin 2

In this Appendix, we list the RG decimation rules in the AF region for both spin- $\frac{3}{2}$  and spin-2 decimations. We also comment on the planar fixed point in both cases.

#### 1. Spin- $\frac{3}{2}$

The RG decimation rules in the AF region are given by

$$\tilde{K}_{14}^{(1)} = 15 \frac{K_1^{(1)} K_3^{(1)}}{6K_2^{(1)} - 90K_2^{(2)} + 441K_2^{(3)}}, \quad (C1)$$

$$\tilde{K}_{14}^{(2)} = -10 \frac{K_1^{(2)} K_3^{(2)}}{4K_2^{(1)} - 40K_2^{(2)} + 49K_2^{(3)}}, \quad (C2)$$

$$\tilde{K}_{14}^{(3)} = \frac{35}{2} \frac{K_1^{(3)} K_3^{(3)}}{8K_2^{(1)} - 20K_2^{(2)} + 63K_2^{(3)}}. \quad (C3)$$

#### 2. Spin 2

The RG equations for a decimation of a spin-2 pair at the AF region are

$$\tilde{K}_{1,4}^{(1)} = \frac{16K_1^{(1)} K_3^{(1)}}{4K^{(1)} - 21 [5K^{(2)} - 56K^{(3)} + 270K^{(4)}]}, \quad (C4)$$

$$\tilde{K}_{1,4}^{(2)} = -\frac{28K_1^{(2)} K_3^{(2)}}{4K^{(1)} - 85K^{(2)} + 616K^{(3)} - 810K^{(4)}}, \quad (C5)$$

$$\tilde{K}_{1,4}^{(3)} = \frac{112K_1^{(3)} K_3^{(3)}}{8K^{(1)} - 110K^{(2)} + 252K^{(3)} - 1215K^{(4)}}, \quad (C6)$$

$$\tilde{K}_{1,4}^{(4)} = -\frac{378K_1^{(4)} K_3^{(4)}}{5 [8K^{(1)} - 30K^{(2)} + 252K^{(3)} - 675K^{(4)}]}, \quad (C7)$$

The method to find planar fixed points is similar to the one we have used for the spin- $\frac{3}{2}$  chain in the main text. The solutions are shown in Table IV and represented as black circles in Fig. 8.

Finally, defining  $s^{(i)} = \frac{K^{(i)}}{K^{(1)}}$ , the globally unstable point in the AF region of the 2-sphere of the  $K^{(1)} \times K^{(2)} \times K^{(3)}$  space is

$$\hat{s}^{(2)*} = -\frac{4}{1617} (55 + 2\sqrt{1969}), \quad (C8)$$

$$\hat{s}^{(3)*} = \frac{1}{6468} (253 + 5\sqrt{1969}). \quad (C9)$$

It is represented as a pink circle in Fig. 8.

### Appendix D: Generating SU(N)-invariant Hamiltonians using spin operators

In this Appendix, we find which SU(2)-symmetric spin- $S$  Hamiltonians of the form (1) are also explicitly invariant under SU( $N$ ) transformations. The idea is to fine-tune the parameters in Eq. (1) in order to match the spectra of SU( $N$ )-symmetric spin Hamiltonians. Notice that this task can be accomplished by considering just the two-site Hamiltonian.

From the dimension of the Hilbert space of a spin  $S$  in Eq. (1) that  $N$  must be equal to  $2S + 1$ . This leaves us with two possibilities: either all the SU( $N$ ) spin operators are the generators of the fundamental representation of the SU( $N$ ) group, or the SU( $N$ ) spin operators at odd (even) sites are the generators of the fundamental (anti-fundamental) representation of the group.

#### a. Fundamental and antifundamental representation on alternating sites

Consider the 2-site problem  $h_{N-\bar{N}}^{\text{SU}(N)} = \mathbf{\Gamma}_2 \cdot \bar{\mathbf{\Gamma}}_3$ , where  $\mathbf{\Gamma} = (\Gamma^{(1)}, \dots, \Gamma^{(N^2-1)})$  and  $\bar{\mathbf{\Gamma}} = (\bar{\Gamma}^{(1)}, \dots, \bar{\Gamma}^{(N^2-1)})$ , with  $\Gamma^{(a)}$  ( $\bar{\Gamma}^{(a)}$ ) being a generator of the fundamental (anti-fundamental) representation of the SU( $N$ ) group. The Clebsch-Gordan series is simply  $N \otimes \bar{N} = 1 \oplus (N^2 - 1)$ . Notice the spectrum is very simple. It has two states, of which one is an SU( $N$ ) singlet, which must correspond to the SU(2) singlet, with zero total spin  $|\tilde{S} = 0\rangle$ . The energy difference can be obtained via the Casimir of the corresponding Young tableau (which can be found, e. g., in Ref. 9) but this knowledge is of no importance here. We now want to recover this spectrum with a spin- $S$  Hamiltonian. Naturally, it must read, up to a constant,

$$h_{N-\bar{N}}^{\text{SU}(N)} = 0 \times P_0 + \Delta E (1 - P_0), \quad (D1)$$

$$= -\Delta E P_0 + \text{const.}, \quad (D2)$$

where  $P_0$  is the projector onto the singlet as defined in Eq. (10) and  $\Delta E$  is the energy difference between the singlet and all the other degenerate levels.

How does this translate to the spin-spin couplings in the Hamiltonian (1)? This is given by Eq. (10). Here, we simply list a few examples. Defining the vector  $\alpha_{N,S} = (\alpha^{(1)}, \dots, \alpha^{(2S)})$ , some spin- $S$   $SU(N)$ -symmetric cases are  $\alpha_{N=3,S=1} = (0, -1)$ ,  $\alpha_{N=4,S=\frac{3}{2}} = (-93, 20, 16)$ , and  $\alpha_{N=5,S=2} = (60, 17, -4, -1)$ . Evidently,  $-\alpha_{N,S}$  yields a Hamiltonian which possesses the same symmetry but represents the FM case.

It is also interesting to recast these Hamiltonians in terms of the ISTs defined in Eq. (5). It can be done by directly using the dictionary between the  $\alpha$ -couplings and the  $K$ -couplings. For instance, in obvious notation,  $\mathbf{K}_{N=3,S=1} = (1, -\frac{4}{5})$ ,  $\mathbf{K}_{N=4,S=\frac{3}{2}} = (1, -\frac{1}{3}, \frac{4}{21})$ , and  $\mathbf{K}_{N=5,S=2} = (1, -\frac{4}{21}, \frac{1}{21}, -\frac{4}{189})$ .

We would like to show now that these Hamiltonians lie inside the AF hyper-octant, as discussed in Sec. (V A). For that, we will derive a more general approach. Let us start by decomposing the projector  $P_0$  as

$$-P_0 = \sum_J \phi_J(S) \hat{O}_J(\mathbf{S}_2, \mathbf{S}_3), \quad (\text{D3})$$

where  $S_2 = S_3 = S$ , and find the coefficients  $\phi_J(S)$ . We are going to compute the matrix elements of the above equation in states of total angular momentum  $\tilde{S}$ , that is, the multiplet coming from the sum of angular momenta  $S_2$  with  $S_3$ , denoted by  $|\tilde{S}, \tilde{M}\rangle = |S_2 S_3; \tilde{S}, \tilde{M}\rangle$ . The matrix element of the  $\hat{O}_J$  operator is found from Ref. 23 (page 111) to be given by

$$\begin{aligned} \langle J' M' | \hat{O}_J | J'' M'' \rangle &= (-1)^{2S+J''} \delta_{J', J''} \delta_{M', M''} \begin{Bmatrix} J'' & S & S \\ J & S & S \end{Bmatrix} \\ &\times |\langle S || Y_J(\mathbf{S}) || S \rangle|^2. \end{aligned} \quad (\text{D4})$$

where  $\{\dots\}$  is Wigner's 6- $j$  symbol. The reduced matrix element of  $Y_J(\mathbf{S})$ ,  $\langle S || Y_J(\mathbf{S}) || S \rangle$ , was calculated in Eq. (B15). Since  $\langle \tilde{S}, \tilde{M} | P_0 | \tilde{S}, \tilde{M} \rangle = \delta_{\tilde{S}, 0}$ , the matrix elements of Eq. (D3) in the  $|\tilde{S}, \tilde{M}\rangle$  states yield

$$(-1)^{2S+\tilde{S}+1} \delta_{\tilde{S}, 0} = \sum_J \phi_J \begin{Bmatrix} \tilde{S} & S & S \\ J & S & S \end{Bmatrix} |\langle S || Y_J(\mathbf{S}) || S \rangle|^2. \quad (\text{D5})$$

Multiplying Eq. (D5) by  $(2\tilde{S}+1) \begin{Bmatrix} J'' & S & S \\ \tilde{S} & S & S \end{Bmatrix}$ , summing over  $\tilde{S}$ , and using the orthogonality relation (page 96 of Ref. 23)

$$\sum_{\tilde{S}} (2\tilde{S}+1) \begin{Bmatrix} \tilde{S} & S & S \\ J & S & S \end{Bmatrix} \begin{Bmatrix} J'' & S & S \\ \tilde{S} & S & S \end{Bmatrix} = \frac{\delta_{J, J''}}{(2J''+1)}, \quad (\text{D6})$$

we find

$$\sum_{\tilde{S}} (-1)^{2S+\tilde{S}+1} \delta_{\tilde{S}, 0} \begin{Bmatrix} \tilde{S} & S & S \\ J'' & S & S \end{Bmatrix} = \frac{|\langle S || Y_J(\mathbf{S}) || S \rangle|^2}{(2J''+1)} \quad (\text{D7})$$

Since  $\begin{Bmatrix} 0 & S & S \\ J'' & S & S \end{Bmatrix} = \frac{(-1)^{J''+2S}}{2S+1}$  (page 98 of Ref. 23), we obtain finally

$$\phi_J(S) = \frac{(-1)^{J+1}}{|\langle S || Y_J(\mathbf{S}) || S \rangle|^2} \frac{(2J+1)}{(2S+1)}. \quad (\text{D8})$$

The most important feature of Eq. (D8) is that it alternates sign with  $J$ . This guarantees that the  $SU(N)$ -symmetric Hamiltonian is in a region in parameter space where the product  $(-1)^{J+1} K_J$  is always positive, i.e., in the middle of the AF hyper-octant (see Fig. 3). Besides, as this large symmetry is preserved along the RG flow, it also corresponds to a fixed point in the middle of the AF hyper-octant, which is totally unstable. Since, as mentioned in the main text, the random singlets generated by the RG process are the same in the entire AF hyper-octant, we conclude that they are all also  $SU(N)$  singlets.

#### b. Fundamental representation on all sites

We now repeat the same steps above for the 2-site problem  $h_{N-N}^{\text{SU}(N)} = \mathbf{\Gamma}_2 \cdot \mathbf{\Gamma}_3$ . As before, the spectrum also has two states but with a different degeneracy. From the Clebsch-Gordan series, we have

$$\begin{aligned} N \otimes N &= \frac{N(N-1)}{2} \oplus \frac{N(N+1)}{2} \\ &= S(2S+1) \oplus (2S+1)(S+1). \end{aligned} \quad (\text{D9})$$

It can be checked that this spectrum can be generated, up to a constant, by

$$h_{N-N}^{\text{SU}(N)} = - \sum_{J=0}^{2S} \left(1 - (-1)^{J+2S}\right) P_J,$$

where  $P_J$  is the projector onto the multiplet of total angular momentum  $J$  [see Eq. (10)]. Notice that if  $S$  is integer (semi-integer), then only the projectors onto the odd (even)  $J$  multiplets are included. Even though there are other ways of reproducing the spectrum for particular values of  $S$  (e. g.,  $S = 2$ ), this is the only choice that does so for generic spin values and, indeed, the one that realizes the  $SU(N)$  symmetry.

As in the  $N - \tilde{N}$  case, we can use Eq. (10) in order to find the corresponding Hamiltonian in the form (1) in terms of spin operators. Some examples are  $\alpha_{N=3,S=1} = (1, 1)$ ,  $\alpha_{N=4,S=\frac{3}{2}} = (-81, 44, 16)$ ,

and  $\alpha_{N=5,S=2} = (-90, -13, 6, 1)$ . They correspond to  $\mathbf{K}_{N=3,S=1} = (1, \frac{4}{5})$ ,  $\mathbf{K}_{N=4,S=\frac{3}{2}} = (1, \frac{1}{3}, \frac{4}{21})$ , and  $\mathbf{K}_{N=5,S=2} = (1, \frac{4}{21}, \frac{1}{21}, \frac{4}{189})$ . Note the similarities with the  $N - \bar{N}$  case: only the signs of the even-rank couplings are reversed.

As in the previous case, by using Eq. (5), the Hamiltonian can be rewritten in terms of ISTs. The generators of the fundamental representation of the  $SU(N)$  group are  $N^2 - 1$   $N \times N$  traceless hermitian matrices. We choose them to satisfy the trace condition

$$\text{Tr}(\Lambda_i \Lambda_j) \propto \delta_{i,j}. \quad (\text{D10})$$

There are  $2J + 1$  linearly independent components for each rank- $J$  IST. By collecting all of them (except for  $J = 0$ ), the number of linear independent ISTs up to order  $2S$  is

$$\sum_{J=1}^{2S} (2J + 1) = 2S(2S + 1) + 2S \quad (\text{D11})$$

$$= 4S(S + 1), \quad (\text{D12})$$

which is exactly  $N^2 - 1$ , with  $N = 2S + 1$ . The  $J = 0$  IST was excluded because its trace is non-zero. The proper choice of the  $SU(N)$  generators is found by combining the ISTs of same rank and components  $M$  and  $-M$ , namely,

$$\Lambda_{J,M} \propto \begin{cases} Y_{J,M}(\mathbf{S}) + Y_{J,-M}(\mathbf{S}), & M > 0, \\ Y_{J,0}(\mathbf{S}), & M = 0, \\ Y_{J,M}(\mathbf{S}) - Y_{J,-M}(\mathbf{S}), & M < 0. \end{cases} \quad (\text{D13})$$

When the linear combination with minus sign is taken, the overall constant is an imaginary number. The above  $\Lambda_{J,M}$  matrices are hermitian, traceless and also linearly independent, since, by construction, the ISTs are linearly independent. This shows that the set of matrices in Eq. (D10) are generators of the fundamental representation of the  $SU(N)$  group.

The trace orthogonality condition Eq. (D10) is also satisfied. In order to show that, we start by expanding a product of two ISTs as a linear combination of ISTs (page 69 of Ref. 23)

$$Y_{J,M}(\mathbf{S}) Y_{J',M'}(\mathbf{S}) = \sum_{J'',M''} \zeta(J, J', J'') \times \langle JJ'; JM | JJ'; MM' \rangle Y_{J'',M''}(\mathbf{S}), \quad (\text{D14})$$

where  $\zeta(J, J', J'')$  does not depend on the tensor components, and the sum over  $J''$  runs from  $|J - J'|$  to  $J + J'$ . The trace involves the computation of diagonal elements of the above equation

$$\begin{aligned} \langle SM | Y_{J,M}(\mathbf{S}) Y_{J',M'}(\mathbf{S}) | SM \rangle \\ = \sum_{J'',M''} \langle JJ'; J''M'' | JJ'; MM' \rangle \\ \times \langle SM | Y_{J'',M''}(\mathbf{S}) | SM \rangle. \end{aligned} \quad (\text{D15})$$

From the Wigner-Eckart theorem, Eq. (B1), the only value of  $M''$  that survives the sum is  $M'' = 0$ , and the Clebsch-Gordan coefficient then requires  $M' = -M$ . Thus,

$$\begin{aligned} \text{Tr}(Y_{J,M}(\mathbf{S}) Y_{J',-M}(\mathbf{S})) = \\ \sum_{J''=|J-J'|}^{J+J'} \langle JJ'; J''0 | JJ'; M - M \rangle \text{Tr}(Y_{J'',0}(\mathbf{S})). \end{aligned} \quad (\text{D16})$$

But only  $Y_{0,0}(\mathbf{S})$  has a non-vanishing trace. Therefore, the only term that survives in the sum is  $J'' = 0$ . But  $J'' = 0$  requires  $J = J'$ . It follows that only  $Y_{J,M}(\mathbf{S}) Y_{J,-M}(\mathbf{S})$  has a non-zero trace. Let us assume, for concreteness, that  $M, M' > 0$ . The other cases follow analogously. Then,

$$\begin{aligned} \text{Tr}(\Lambda_{J,M} \Lambda_{J',M'}) \propto \text{Tr}(Y_{J,M}(\mathbf{S}) + Y_{J,-M}(\mathbf{S})) \times \\ (Y_{J',M'}(\mathbf{S}) + Y_{J',-M'}(\mathbf{S})), \end{aligned} \quad (\text{D17})$$

$$\propto 2\delta_{J,J'} (\delta_{M,M'} + \delta_{M,-M'}). \quad (\text{D18})$$

Therefore, the trace condition  $\text{Tr}(\Lambda_{J,M} \Lambda_{J',M'}) \propto \delta_{J,J'} \delta_{M,M'}$  is satisfied by the operators defined in Eq. (D13). We have thus proved all the conditions that are necessary in order that the collection of the  $N^2 - 1$  traceless ISTs of rank up to  $2S$  (excluding zero rank) can be chosen as generators of the fundamental representation of the  $SU(N)$  group.

## Appendix E: When the two-spin Hamiltonian has a singlet ground state

Fundamental to our understanding of the  $\psi = \frac{1}{2}$  AF phases is the fact that singlets are formed in the decimations on some of the semi-axes. In this Appendix, we analyze in detail the conditions under which the ground state of the two-spin problem  $S_2 = S_3 = S$  is a singlet. We focus on a given axis and, therefore, only ISTs of a given rank, say  $J$ , are non-zero.

The energy of a multiplet of total angular momentum  $J'$ ,  $E_J(J')$ , can be found by using Eq. (D4) in a generic eigenstate of the Hamiltonian,  $|SS; J'M'\rangle$

### 1. On the $K^{(3)} < 0$ semi-axis

$$E_J(J') = \left\langle SS; J'M' \left| \hat{O}_J \right| SS; J'M' \right\rangle \quad (\text{E1})$$

$$= (-1)^{2S+J'} \left\{ \begin{matrix} J' & S & S \\ J & S & S \end{matrix} \right\} |\langle S || Y_J(\mathbf{S}) || S \rangle|^2 \quad (\text{E2})$$

Note that, since the operator is SU(2)-symmetric, the right-hand side is the energy of the system, independent of  $M'$ . One can use Eq. (B15) to compute the reduced matrix element but, for now, we just note that it is a function of only  $J$  and  $S$ , assumed to be fixed in this analysis. We define the ratio

$$\tilde{E}_J(J') = \frac{E_J(J')}{(-1)^{2S} |\langle S || Y_J(\mathbf{S}) || S \rangle|^2}$$

$$= (-1)^{J'} \left\{ \begin{matrix} J' & S & S \\ J & S & S \end{matrix} \right\}. \quad (\text{E3})$$

The task is to find the value of  $J'$  that minimizes (maximizes)  $\tilde{E}_J(J')$  for integer (half-integer)  $S$ , with  $J$  varying from 0 to  $2S$ . We have numerically checked up to  $J = 8$  and  $S = 80$  that this requirement is satisfied for  $J' = 0$ . This provides strong evidence that the singlet is the ground state when  $(-1)^J K^{(J)} > 0$ , which is the result quoted in the main text.

### Appendix F: Beyond first-order perturbation theory of degenerate multiplets

We show explicitly how to compute second-order corrections to two concrete cases where the ground multiplet is not a singlet but the first-order perturbation theory renormalization vanishes. The calculations to find such corrections are lengthy and have to be done case by case. We deal with the case where the spins are equal to  $\frac{3}{2}$ . We start by showing the steps to derive the RG renormalization when decimations are performed on the  $K^{(3)} < 0$  axis, where the local ground state is a spin-1 multiplet. The first-order perturbation theory vanishes due to case (a) discussed in Section III 1. After that, we compute second-order effects on spins connected by  $K^{(2)} > 0$  tensors. This is an axis where case (b) of Section III 1 leads to a vanishing first-order renormalization. The question we want to address is whether higher order corrections could give contributions that would change the ground state properties in a non-trivial way. We have checked through numerical diagonalization of the three-site problem that in both cases there are indeed small second-order SU(2)-symmetric interactions with the side spins of a decimated pair.

The four-spin Hamiltonian can be re-written as

$$\mathcal{H} = V_{1,2} + H_{2,3}^0 + V_{3,4} \quad (\text{F1})$$

where  $H^0$  is the unperturbed Hamiltonian. First-order perturbation theory gives the following correction to the Hamiltonian

$$\Delta H^{(1)} = P_{\tilde{S}} V_{1,2} P_{\tilde{S}} + P_{\tilde{S}} V_{3,4} P_{\tilde{S}}, \quad (\text{F2})$$

where  $P_{\tilde{S}}$  is the projector onto the ground multiplet, which in this case is a  $\tilde{S} = 1$  total angular momentum state. Applying the Wigner-Eckart theorem, one can easily show that this correction is zero, since the sum of angular momenta  $S = 1$  and  $S = 3$  cannot give  $\tilde{S} = 1$ . The first order effect would be, therefore, to break the chain into 2 decoupled smaller chains.

A natural question is what is the lowest-order correction that gives a non-zero contribution. The second-order correction is given by

$$\Delta H^{(2)} = P_{\tilde{S}} (V_{1,2} + V_{3,4}) \bar{P} \frac{1}{E_0 - H_{2,3}^0} \bar{P} (V_{1,2} + V_{3,4}) P_{\tilde{S}} \quad (\text{F3})$$

$$= \Delta H_{1,2}^{(2)} + \Delta H_{3,4}^{(2)} + \Delta H_{(1,2),(3,4)}^{(2)} \quad (\text{F4})$$

where  $\bar{P} = 1 - P_{\tilde{S}}$  and we have defined

$$\Delta H_{i,i+1}^{(2)} = P_{\tilde{S}} V_{i,i+1} \bar{P} \frac{1}{E_0 - H_{2,3}^0} \bar{P} V_{i,i+1} P_{\tilde{S}}, \quad (\text{F5})$$

$$\Delta H_{(1,2),(3,4)}^{(2)} = P_{\tilde{S}} V_{1,2} \bar{P} \frac{1}{E_0 - H_{2,3}^0} \bar{P} V_{3,4} P_{\tilde{S}} + \text{H.c.} \quad (\text{F6})$$

We first consider  $\Delta H_{(1,2),(3,4)}^{(2)}$ . It gives rise to different types of terms which we call  $\Delta \mathcal{V}_{J,\tilde{M}}$ , where  $J$  and  $\tilde{M}$  correspond to the rank and component of the IST of  $\tilde{\mathbf{S}}$  it contains. There is a next-nearest-neighbor ferromagnetic interaction independent of  $\tilde{\mathbf{S}}$  ( $J = \tilde{M} = 0$ )

$$\Delta \mathcal{V}_{0,0} = -\frac{23\sqrt{\pi}}{35} \hat{O}_3(\mathbf{S}_1, \mathbf{S}_4). \quad (\text{F7})$$

The other terms are genuine three-body interactions given by



$\tilde{M}$	$\alpha_M^{(\tilde{M})}$
0	$\frac{1}{\sqrt{3}} (3, -2, 1, 0, -1, 2, -3)$
1	$\frac{1}{\sqrt{3}} (\sqrt{3}, -\sqrt{5}, \sqrt{6}, -\sqrt{6}, \sqrt{5})$
$\tilde{M}$	$\beta_M^{(\tilde{M})}$
0	$\frac{8}{\sqrt{5}} (-5, 0, 3, -4, 3, 0, -5)$
1	$\frac{8}{\sqrt{5}} (-5, \sqrt{15}, -\sqrt{2}, -\sqrt{2}, \sqrt{15}, -5)$
2	$\frac{16}{\sqrt{10}} (-\sqrt{5}, \sqrt{10}, -\sqrt{12}, \sqrt{10}, -\sqrt{5})$

Table V. Constants that appear in the three-body interaction terms of Eqs. (F8) and (F9). The vector components correspond to the  $M$  index, starting at  $M = -3$ .

$$\Delta\mathcal{V}_{1,\tilde{M}} = \frac{\sqrt{\pi}}{35} \sum_{M=-3}^{3-\tilde{M}} \alpha_M^{(\tilde{M})} Y_{3,M}(\mathbf{S}_1) Y_{1,\tilde{M}}(\tilde{\mathbf{S}}) Y_{3,-M-\tilde{M}}(\mathbf{S}_4) + \text{H.c.}, \quad (\text{F8})$$

$$\Delta\mathcal{V}_{2,\tilde{M}} = \frac{\sqrt{\pi}}{35} \sum_{M=-3}^{3-\tilde{M}} \beta_M^{(\tilde{M})} Y_{3,M}(\mathbf{S}_1) Y_{2,\tilde{M}}(\tilde{\mathbf{S}}) Y_{3,3-\tilde{M}}(\mathbf{S}_4) + \text{H.c.} \quad (\text{F9})$$

In Eq. (F8),  $\tilde{M}$  runs from  $-1$  to  $1$ , whereas in Eq. (F9) the sum is from  $-2$  to  $2$ . The coefficients  $\alpha_M^{(\tilde{M})}$  and  $\beta_M^{(\tilde{M})}$  are given in Table V. Through numerical diagonalization of 4-site chains, we find that all the terms  $\Delta\mathcal{V}_{J,\tilde{M}}$  are *non-frustrating*, i. e., the ground state is the same whether we keep them in the RG procedure or not. For this reason, we will neglect them in what follows.

We keep, however, the  $\Delta H_{i,i+1}^{(2)}$  terms. For  $i = 1$ , for example,

$$\frac{\Delta H_{1,2}^{(2)}}{K_1^{(J)}} = \sum_{\{M_1, M_2\}=-J}^J (-1)^{M_1-M_2} [Y_{JM_1}(\mathbf{S}_1) Y_{J-M_2}(\mathbf{S}_1)] \times \left[ PY_{J-M_1}(\mathbf{S}_2) \tilde{P} \frac{1}{E_0 - H_{2,3}^0} \tilde{P} Y_{JM_2}(\mathbf{S}_2) P \right]. \quad (\text{F10})$$

The term  $Y_{JM_1}(\mathbf{S}_1) Y_{J-M_2}(\mathbf{S}_1)$  can be decomposed as a linear combination that conserves the azimuthal component of the angular momentum, the same as in Eq. (D14) of Appendix (D). For example, for  $J = 3$  and  $M_1 = M_2 = -3$ ,

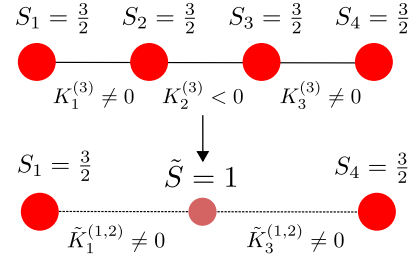


Figure 10. (Color online) RG step when the spins are equal to  $\frac{3}{2}$  and  $K^{(3)} < 0$ . The 2-spin ground-state multiplet is  $\tilde{S} = 1$  and the first-order perturbation theory yields a vanishing renormalization. Unlike in the cases discussed in Section III 1, the second-order step generates tensors of ranks that were not present in the original chain.

$$Y_{3,-3}(\mathbf{S}_1) Y_{3,3}(\mathbf{S}_1) = -\frac{315}{32\sqrt{\pi}} Y_{0,0}(\mathbf{S}_1) + \frac{63}{16} \sqrt{\frac{3}{\pi}} Y_{1,0}(\mathbf{S}_1) - \frac{21}{16} \sqrt{\frac{5}{\pi}} Y_{2,0}(\mathbf{S}_1) + \frac{3}{8} \sqrt{\frac{7}{\pi}} Y_{3,0}(\mathbf{S}_1). \quad (\text{F11})$$

The projection onto the ground state multiplet also conserves the  $M$  values and, therefore, can be decomposed in terms of ISTs of the effective new degrees of freedom,

$$PY_{J-M_1}(\mathbf{S}_2) \tilde{P} \frac{1}{E_0 - H_{2,3}^0} \tilde{P} Y_{JM_2}(\mathbf{S}_2) P = \frac{1}{K_2^{(3)}} \sum_{J'} \beta_{J',(M_2-M_1)} Y_{J',(M_2-M_1)}(\tilde{\mathbf{S}} = 1). \quad (\text{F12})$$

Plugging this decomposition into Eq. (F10), we find

$$PV_{1,2} \tilde{P} \frac{1}{E_0 - H_{2,3}^0} \tilde{P} V_{1,2} P = \frac{(K_1^{(3)})^2}{|K_2^{(3)}|} \sum_{J=0}^2 \gamma_J \hat{O}_J \left( \mathbf{S}_1 = \frac{3}{2}, \tilde{\mathbf{S}} = 1 \right). \quad (\text{F13})$$

For this particular case,

$$\gamma_0 = \frac{2079}{128}, \quad \gamma_1 = \frac{63}{20}, \quad \gamma_2 = \frac{189}{100}. \quad (\text{F14})$$

Neglecting the constant factor, we find the residual 2-body interaction between the effective  $\tilde{S} = 1$  spin and the  $S_1 = \frac{3}{2}$  spin

$$\Delta H_{1,2}^{(2)} = \frac{(K_1^{(3)})^2}{|K_2^{(3)}|} \left( \frac{63}{20} \hat{O}_1 + \frac{189}{100} \hat{O}_2 \right), \quad (\text{F15})$$

where  $\hat{O}_i = \hat{O}_i(\mathbf{S}_1 = \frac{3}{2}, \tilde{\mathbf{S}} = 1)$ . By symmetry, we obtain the coupling connecting to site 4 by replacing  $1 \leftrightarrow 4$ . Note that the decimation generates couplings between ISTs that were not coupled in the initial Hamiltonian ( $\hat{O}_1$  and  $\hat{O}_2$ ). A schematic representation of the RG rule Eq. (F15) is represented in Fig. 10. As explained in Fig. 11, although the first steps yield a non-zero renormalization of couplings, in later steps the RG procedure breaks the chain into two parts.

## 2. On the $K^{(2)} > 0$ semi-axis

In this case, the reason why the first-order calculation vanishes is that the couplings constants are proportional to the following 6- $j$  symbol

$$\left\{ \begin{array}{ccc} 2 & 2 & 2 \\ \frac{3}{2} & \frac{3}{2} & \frac{3}{2} \end{array} \right\} = 0. \quad (\text{F16})$$

The steps of this calculation are analogous to the previous case. The decomposition of  $Y_{2,M_1}(\mathbf{S}_1) Y_{2,-M_2}(\mathbf{S}_1)$  gives terms with  $J$  ranging from 0 to 3, except  $J = 2$ . The effective Hamiltonian that connects a spin  $S_1 = \frac{3}{2}$  with a spin  $\tilde{S} = 2$  is, up to an additive constant,

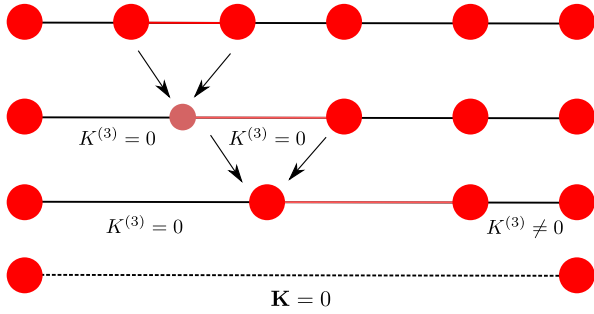


Figure 11. (Color online) Schematic representation of the RG decimations after the decimation procedure shown in this Appendix is implemented, and the generation of zero couplings after some RG time. The strongest coupled pair is represented by the red line. The first decimation generates an effective spin  $\tilde{S} = 1$  (light red), that is coupled to its neighbors via  $K^{(1,2)}$ , but not  $K^{(3)}$ . The second decimation leads back to an effective spin  $\frac{3}{2}$ , with its left neighbor having  $K^{(3)} = 0$ . The third decimation is a second-order singlet-formation decimation and the final effective coupling of the edge spins is zero. This is so because  $\tilde{K}^{(J)}$  involves the product of neighboring couplings of same rank and, whereas the right neighbor has only  $K^{(3)} \neq 0$ , the left neighbor has  $K^{(3)} = 0$ .

$$\Delta H_{1,2}^{(2)} = \frac{(K_1^{(2)})^2}{K_2^{(2)}} \left( \frac{9}{16} \hat{O}_1 - \frac{3}{56} \hat{O}_3 \right). \quad (\text{F17})$$

Here,  $\hat{O}_i = \hat{O}_i(\mathbf{S}_1 = \frac{3}{2}, \tilde{\mathbf{S}} = 2)$ . As in the previous subsection, this procedure generates an RG flow with non-zero couplings in the first steps, but vanishing couplings are generated later via the same mechanism as the one described in Fig. 11. Also analogous to the previous section are the calculations of all the three-body and long-ranged effective couplings.

- 
- <sup>1</sup> P. A. Lee and T. V. Ramakrishnan, *Rev. Mod. Phys.* **57**, 287 (1985).
  - <sup>2</sup> F. Iglói and C. Monthus, *Phys. Rep.* **412**, 277 (2005).
  - <sup>3</sup> T. Vojta, *J. Phys. A: Math. Gen.* **39**, R143 (2006).
  - <sup>4</sup> D. S. Fisher, *Phys. Rev. B* **50**, 3799 (1994).
  - <sup>5</sup> S. k. Ma, C. Dasgupta, and C. k. Hu, *Phys. Rev. Lett.* **43**, 1434 (1979).
  - <sup>6</sup> C. Dasgupta and S.-k. Ma, *Phys. Rev. B* **22**, 1305 (1980).
  - <sup>7</sup> R. N. Bhatt and P. A. Lee, *Phys. Rev. Lett.* **48**, 344 (1982).
  - <sup>8</sup> K. Damle and D. A. Huse, *Phys. Rev. Lett.* **89**, 277203 (2002).
  - <sup>9</sup> J. A. Hoyos and E. Miranda, *Phys. Rev. B* **70**, 180401 (2004).
  - <sup>10</sup> L. Fidkowski, H.-H. Lin, P. Titum, and G. Refael, *Phys. Rev. B* **79**, 155120 (2009).
  - <sup>11</sup> V. L. Quito, J. A. Hoyos, and E. Miranda, *Phys. Rev. Lett.* **115**, 167201 (2015).
  - <sup>12</sup> A. Imambekov, M. Lukin, and E. Demler, *Phys. Rev. A* **68**, 063602 (2003).
  - <sup>13</sup> C. Wu, J.-p. Hu, and S.-c. Zhang, *Phys. Rev. Lett.* **91**, 186402 (2003).
  - <sup>14</sup> J. J. García-Ripoll, M. A. Martin-Delgado, and J. I. Cirac, *Phys. Rev. Lett.* **93**, 250405 (2004).
  - <sup>15</sup> C. Wu, *Mod. Phys. Lett. B* **20**, 1707 (2006).
  - <sup>16</sup> M. A. Cazalilla, A. F. Ho, and M. Ueda, *New J. Phys.* **11**, 103033 (2009).
  - <sup>17</sup> A. V. Gorshkov, M. Hermele, V. Gurarie, C. Xu, P. S. Julienne, J. Ye, P. Zoller, E. Demler, M. D. Lukin, and A. M. Rey, *Nature Phys.* **6**, 289 (2010).
  - <sup>18</sup> X. Zhang, M. Bishof, S. L. Bromley, C. V. Kraus, M. S. Safronova, P. Zoller, A. M. Rey, and J. Ye, *Science* **345**, 1467 (2014).
  - <sup>19</sup> F. Scazza, C. Hofrichter, M. Höfer, P. C. De Groot, I. Bloch, and S. S. Fölling, *Nature Phys.* **10**, 779 (2014).
  - <sup>20</sup> S. Taie, R. Yamazaki, S. Sugawa, and Y. Takahashi, *Nature Phys.* **8**, 825 (2012).
  - <sup>21</sup> E. Westerberg, A. Furusaki, M. Sigrist, and P. A. Lee, *Phys. Rev. B* **55**, 12578 (1997).
  - <sup>22</sup> K. Yang and R. N. Bhatt, *Phys. Rev. Lett.* **80**, 4562 (1998).
  - <sup>23</sup> A. R. Edmonds, *Angular Momentum in Quantum Mechanics* (Princeton University Press, 1996).
  - <sup>24</sup> C. V. Ciobanu, S.-K. Yip, and T.-L. Ho, *Phys. Rev. A* **61**, 033607 (2000).
  - <sup>25</sup> S. Alexander and J. Bernasconi, *Journal of Physics C: Solid State Physics* **12**, L1 (1979).
  - <sup>26</sup> T. A. L. Ziman, *Phys. Rev. Lett.* **49**, 337 (1982).
  - <sup>27</sup> G. Theodorou, *Journal of Physics C: Solid State Physics* **15**, L1315 (1982).
  - <sup>28</sup> M. Cieplak and G. Ismail, *Journal of Physics C: Solid State Physics* **20**, 1309 (1987).
  - <sup>29</sup> S. Evangelou and D. Katsanos, *Physics Letters A* **164**, 456 (1992).
  - <sup>30</sup> T. Hikihara, A. Furusaki, and M. Sigrist, *Phys. Rev. B* **60**, 12116 (1999).
  - <sup>31</sup> J. A. Hoyos, *Phys. Rev. E* **78**, 032101 (2008).
  - <sup>32</sup> G. Refael, S. Kehrein, and D. S. Fisher, *Phys. Rev. B* **66**, 060402 (2002).
  - <sup>33</sup> A. Saguia, B. Boechat, and M. A. Continentino, *Phys. Rev. B* **68**, 020403 (2003).
  - <sup>34</sup> E. Carlon, P. Lajkó, H. Rieger, and F. Iglói, *Phys. Rev. B* **69**, 144416 (2004).
  - <sup>35</sup> H. Jones, *Groups, Representations and Physics* (CRC Press, 1998).
  - <sup>36</sup> J. C. Getelina, F. C. Alcaraz, and J. A. Hoyos, *Phys. Rev. B* **93**, 045136 (2016).
  - <sup>37</sup> J. A. Hoyos and E. Miranda, *Phys. Rev. B* **69**, 214411 (2004).